

CHALMERS



An investigation of the dynamic characteristics of a tilting disc check valve using CFD analyses

Master of Science Thesis in the Master Degree Programme, Nuclear Engineering

Linnea Jansson
Josefin Lövmärk

Department of Chemical and biological engineering
Division of Chemical engineering
CHALMERS UNIVERSITY OF TECHNOLOGY
Gothenburg, Sweden, 2013

An investigation of the dynamic characteristics of a
tilting disc check valve using CFD analyses

LINNEA JANSSON AND JOSEFIN LÖVMARK

Department of Chemical and biological engineering
CHALMERS UNIVERSITY OF TECHNOLOGY
Göteborg, Sweden 2013

An investigation of the dynamic characteristics of a tilting disc check valve
using CFD analyses

LINNEA JANSSON, JOSEFIN LÖVMARK

© LINNEA JANSSON, JOSEFIN LÖVMARK, 2013

Department of Chemical and biological engineering
Chalmers University of Technology
SE-41296 Göteborg
Sweden
Telephone +46 (0)31 772 1000

Göteborg, Sweden 2013

Abstract

In this master's thesis, the dynamic characteristics of a tilting disc check valve is investigated in order to determine a closing time, using computational fluid dynamics. A lever arm with a removable weight is attached to the tilting disc check valve. The simulation is done in ANSYS Fluent version 14.5 and the main analyses are to simulate the closure of the tilting disc check valve with and without the removable weight, when the disc starts from its fully opened position. Sensitivity analyses are also performed to investigate the suitability of different settings in ANSYS Fluent. The movement of the disc is described by a user-defined function. The outcome of this master's thesis is that the characteristics of the moving disc in the tilting disc check valve is different between the simulations with and without the removable weight. The closing time is faster when the removable weight is used than for when the weight is removed. The characteristics are different for the two cases. When the weight is removed, the disc starts to close later and the absolute angular velocity during the closing process increases. For the simulation with the removable weight, the disc starts to move earlier but the absolute angular velocity is not monotonically increasing. During the closing process the angular velocity changes sign, this results in a small reopening of the disc before it starts to close again. The results from the computational fluid dynamics simulation need to be evaluated against the results from experiments in order for these results to be fully reliable.

Keywords: CFD, UDF, tilting disc check valve, ANSYS Fluent

Acknowledgement

First, we would like to thank our examiner Professor Bengt Andersson for all his help and support. We also owe many thanks to Johan Andersen, Thomas Probert, and Ronnie Andersson, our supervisors at ÅF, OKG, and Chalmers respectively, for sharing their expertise with us during these months. Furthermore, we would like to extend our sincere gratitude to Paula Svensson at OKG and Göran Bennarsten at ÅF for making this project possible. Last but not least, a big thanks to our families and all the co-workers at ÅF for their support!

Nomenclature

Roman

A	Area
CFL	Courant number
F	Force
g	Gravitational acceleration
h	Enthalpy
I	Moment of inertia
I_t	Turbulent intensity
k	Turbulent kinetic energy
L	Hydraulic diameter
M	Moment
m	Mass
\dot{m}	Mass flow rate
N	Normal force
p	Pressure
P	Mean pressure
p'	Fluctuating pressure
Re	Reynolds number
t	Time
u	Velocity
U	Mean velocity
u'	Fluctuating velocity

Greek

α	Angular acceleration
ε	Dissipation rate
θ	Angle
μ	Dynamic viscosity
μ_k	Coefficient of kinetic friction
μ_s	Coefficient of static friction
μ_t	Dynamic turbulent viscosity
ν	Kinematic viscosity
ν_t	Kinematic turbulent viscosity
ρ	Density
τ	Viscous stresses
ω	Specific dissipation rate
ω	Angular velocity

Abbreviations

CFD	Computational fluid dynamics
FKA	Forsmarks kraftgrupp AB
MUSCL	Monotone Upstream-centred Schemes for Conservation Laws
OKG	Oskarshamns kraftgrupp
QUICK	Quadratic Upstream Interpolation for Convective Kinetics
RAB	Ringhals AB
TVO	Teollisuuden Voima Oyj
UDF	User-defined function

Contents

1	Introduction.....	1
1.1	Background.....	1
1.2	Objectives	1
1.3	Assumptions and limits of applicability	1
2	Theory	3
2.1	Check valves.....	3
2.2	Tilting disc check valve	3
2.2.1	Motion of a tilting disc check valve in a fluid.....	4
2.3	Computational fluid dynamics.....	7
2.3.1	Governing equations of fluid flows.....	7
2.3.2	Turbulence.....	8
2.3.3	Turbulence modelling	8
2.3.4	Eddy viscosity turbulence models.....	10
2.3.5	Near wall modelling	13
2.3.6	Boundary conditions	13
2.3.7	Discretisation schemes	14
2.3.8	Choosing the pressure-velocity coupling algorithm.....	16
2.4	Meshing	16
2.4.1	Dynamic mesh.....	17
2.5	User-defined functions	18
3	Input conditions of the CFD simulation.....	19
3.1	Geometry of the tilting disc check valve	19
3.2	Properties of the tilting disc check valve.....	20
3.3	Properties of the fluid	21
3.4	Boundary conditions.....	21
3.4.1	Inlet boundary condition	21
3.4.2	Outlet boundary condition.....	22
3.4.3	Boundary condition for the turbulent quantities	22
4	Method and application.....	23
4.1	Motion of the tilting disc check valve in a fluid.....	23
4.2	Main analysis	23

4.2.1	Mesh	24
4.2.2	CFD simulation	25
4.3	Sensitivity analysis	26
4.3.1	Mesh	26
4.3.2	Boundary condition	26
4.3.3	Time step size	26
4.3.4	Maximum number of iterations in one time step	26
4.3.5	Discretization scheme	26
4.3.6	Turbulence model.....	27
4.4	UDF	27
5	Results.....	28
5.1	Main analysis	28
5.2	Sensitivity analysis	30
5.2.1	Mesh	30
5.2.2	Boundary condition	31
5.2.3	Time step size	32
5.2.4	Maximum number of iterations in one time step	32
5.2.5	Discretization scheme	33
5.2.6	Turbulence model.....	33
6	Discussion	36
6.1	Main analysis	36
6.2	Sensitivity analysis	37
6.2.1	Mesh	37
6.2.2	Boundary condition	37
6.2.3	Time step size	38
6.2.4	Maximum number of iterations in one time step	38
6.2.5	Discretization scheme	38
6.2.6	Turbulence model.....	38
7	Conclusion	40
8	Future work.....	41
9	Bibliography	42

1 Introduction

1.1 Background

Check valves are, among other applications, used in nuclear reactors to prevent the flow of fluid in the reverse direction, where safety is the paramount factor. Numerical simulations can be used in order to analyse the flow instead of using physical experiments, which is both costly and time consuming. In Sweden, the one-dimensional program RELAP5 is used to analyse piping systems in the nuclear power plants. In order to improve the RELAP5 models, experiments must be performed to verify the change of the models. The existing RELAP5 models for describing check valves is too conservative and therefore experiments and analysis are performed in order to reduce the conservatism. One experiment will be performed by Beräkningsgruppen, collaboration between OKG, TVO, FKA, and RAB and the Szewalski Institute of Fluid-Flow Machinery of the Polish Academy of Sciences. The main objective of the experiment is to investigate and determine the dynamic characteristics of a tilting disc check valve. This master's thesis is also part of this work as it is a detailed analysis of the dynamic behaviour of the tilting disc check valve. The master's thesis has been performed in collaboration with ÅF, OKG, and Chalmers.

1.2 Objectives

The outcome of this master's thesis will be used and validated with the experimental data. The result will be used to either improve existing or develop new RELAP5 models. The objective of this master's thesis is to investigate the closing time and characteristics for the tilting disc check valve used in the experiments. A sensitivity analysis is performed to investigate the setting in the computational fluid dynamic (CFD) simulations; see chapter 4.3. A literature study is performed to understand the underlying physics and to obtain knowledge of the different programs used during the course of this master's thesis. The simulations are performed in ANSYS Fluent version 14.5 and afterwards, the results are post processed and analysed. A user-defined function (UDF) is generated in order to determine the movement of the tilting disc check valve.

1.3 Assumptions and limits of applicability

The assumptions and limits of applicability of this master's thesis are the following.

1. In the coming experiment, the pump will be shut down (tripping), which will affect the tilting disc check valve and the closing process will begin. In this master's thesis, there is a one-way coupling between the pump and the tilting disc check valve, where the pump is affecting the valve but not the other way around. Therefore, the pump does not need to be modelled but is taken in to account as a boundary condition of the mass flow entering the system.

2. When modelling the geometry of the tilting disc check valve there are some minor simplifications made in order to make it more applicable for CFD calculations and mesh grid generation. For example, a few round edges are converted to sharp edges.
3. The fluid flowing in the system is water. The water is assumed to be in one phase and to be incompressible.
4. The number of cells in the mesh and the size of the chosen time step are restricted because of the computational resources available. This is further investigated in the sensitivity analysis; see chapter 5.2.
5. The maximal opening angle of the disc is 67.2 degrees but it is set to 65 degrees in order to get a better quality of the mesh between the disc and the stopping lug.
6. The frictional forces between the solids in the tilting disc check valve are neglected; see chapter 4.1.
7. The turbulence models applied in this master's thesis is the two equations eddy viscosity turbulence models.
8. The pipes at inlet and outlet of the tilting disc check valve are assumed to have a diameter of 0.121 m and 0.128 m, respectively.

2 Theory

2.1 Check valves

Valves are used in industries to regulate flow and pressure. They are installed in piping systems and they operate in the full range between opened and closed. An open valve is equal to full flow and a closed valve prevents the fluid from flowing. [1] It is important that the right type of valve is installed for a certain application and that the valve is operating properly. There exist several types of valves and one category of them is the check valves. [2] A check valve is a valve that prevents the flow from flowing in the reverse direction. They are used in different industries to prevent damage to systems. They operate on their own and respond automatically to the flow. There are different types of check valves, e.g. lift check valves, split disc check valves, swing check valves, and tilting disc check valves. In this thesis, the investigated valve is a tilting disc check valve.

2.2 Tilting disc check valve

The general design of a tilting disc check valve can be seen in Figure 1. The check valve is seen from the side, with the valve housing surrounding the movable disc and a weighted lever attached to it. The disc is rotating about an axis located in the flow. The solid lines show the valve in closed position and the dotted lines show the valve in fully opened position. [3]

Tilting disc check valves are mainly used in systems where the fluid is in liquid phase but they can also be applied in systems with gas and vapour. [4] The closure of the tilting disc check valve is due to the flow, the weight of the disc, and in some cases due to a weighted lever. [3] Auxiliary springs can be attached to the tilting disc check valves in order to reduce the closing time. An auxiliary spring can contribute to minimize the water hammering phenomena. [4] The tilting disc check valve closes faster than the swing check valve due to the location of the rotational axis. For the tilting disc check valve, the rotational axis is located in the flow instead of above the flow, as is the case for the swing check valve, thus shortening the distance for the disc to travel and hence also its moment of inertia. [2]

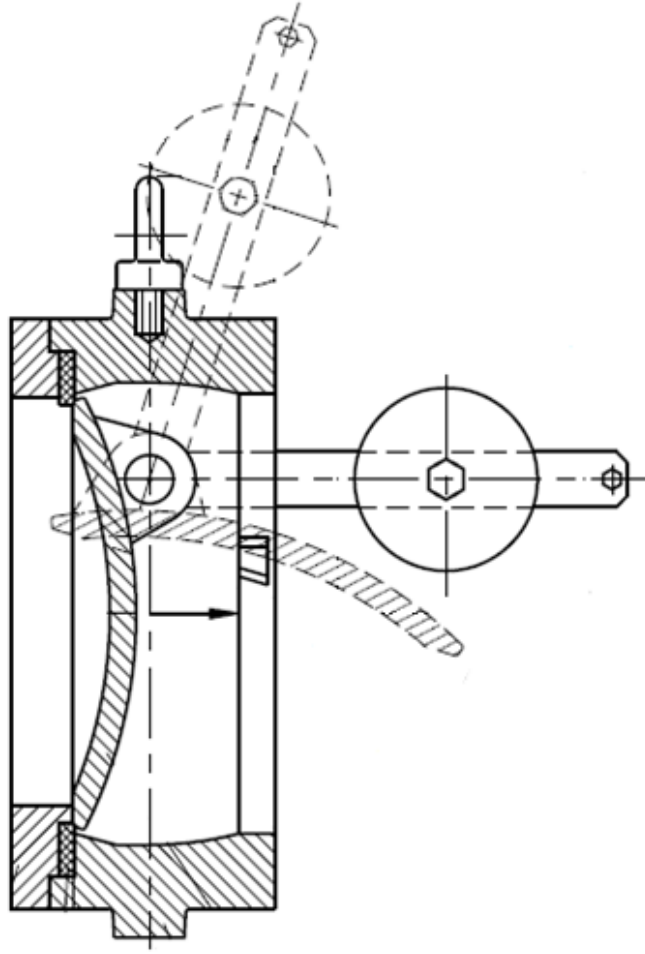


Figure 1: Scheme of the tilting disc check valve used in the experiment.

2.2.1 Motion of a tilting disc check valve in a fluid

The motion of a tilting disc check valve is restricted to angular motion and rotation around a fixed axis. The angular acceleration, α , of the disc can be determined using Newton's second law for fixed axis rotation; see equation (2.1).

$$I_0 \alpha = \sum M_0 \quad (2.1)$$

Here, the moment of inertia, I_0 , and the moments of the forces acting on the disc, M_0 , is calculated about the fixed axis. Because the disc is constrained to move about one axis only, it is enough to calculate the moment of inertia about this axis. The moment of inertia about the fixed axis is calculated as seen in equation (2.2), where r is the shortest distance between the axis, about which the moment of inertia is calculated, and the mass element dm .

$$I_0 = \int r^2 dm \quad (2.2)$$

If the moment of inertia about the centre of mass is known, the moment of inertia about the rotational axis can be calculated using the parallel axis theorem; see equation (2.3). In equation (2.3), I_{cm} is the moment of inertia about the centre of mass, m is the mass of the

object, and d is the perpendicular distance between the centre of mass of the object and the rotational axis.

$$I_0 = I_{cm} + md^2 \quad (2.3)$$

The moments about the fixed axis is calculated by the cross product between the force vectors, \mathbf{F} , acting on the disc and their respective position vectors, as seen in equation (2.4). The position vector \mathbf{r} is the vector describing the shortest distance from the fixed axis to the point at which the force is applied. To calculate the total moment about the fixed axis, all forces acting on the disc needs to be determined.

$$M_{tot} = \sum M_0 = \sum \mathbf{r} \times \mathbf{F} \quad (2.4)$$

A tilting disc check valve is constructed so the weight of the disc will operate in order to close the valve. This means that without any external forces applied to the disc, the tilting disc check valve will be closed. The force on the disc due to gravity can be seen in equation (2.5).

$$F_{gravity} = m_{disc}g \quad (2.5)$$

The gravitational force is applied at the centre of mass of the disc, so that when calculating the moment due to gravity, the position vector \mathbf{r}_{cm} describes the shortest distance between the centre of mass and the fixed axis. If the system consists of more than one part, the position vector for the common centre of mass can be calculated according to equation (2.6), where m_i and \mathbf{r}_i is the mass and the coordinates, for the centre of mass for the different objects, and m_{tot} is the total mass of the system.

$$\mathbf{r}_{cm} = \frac{1}{m_{tot}} \sum_{i=1}^n m_i \mathbf{r}_i \quad (2.6)$$

The moment due to the gravitational forces around the fixed axis are thus calculated as in equation (2.7), where $\hat{\mathbf{n}}$ is aligned with the rotational axis.

$$M_{gravity} = (\mathbf{r}_{cm} \times \mathbf{F}_{gravity}) \cdot \hat{\mathbf{n}} \quad (2.7)$$

Frictional forces will occur between the solid parts of the tilting disc check valve which can rotate and which is in contact with another solid surface. Before the tilting disc check valve starts to move, the maximum static frictional forces that occur between the surfaces are described by equation (2.8), where μ_s is the coefficient of static friction and N is the normal force. When the tilting disc check valve starts to move, the frictional forces can be calculated using equation (2.9), where μ_k is the coefficient of kinetic friction.

$$F_{friction,s} = \mu_s N \quad (2.8)$$

$$F_{friction,k} = \mu_k N \quad (2.9)$$

The moment due to frictional forces around the fixed axis are thus calculated as in equation (2.7).

$$M_{friction} = (\mathbf{r}_{cm} \times \mathbf{F}_{friction}) \cdot \hat{\mathbf{n}} \quad (2.10)$$

The forces acting on the disc due to the movement of the surrounding fluid are pressure forces and viscous forces. The pressure forces are calculated by taking the pressure on a face and multiplying it with the area of the face, as can be seen in equation (2.11).

$$F_{pressure} = p dA \quad (2.11)$$

To calculate the total momentum about the fixed axis due to pressure forces, the cross product between the pressure force vector and the position vector is summed for all faces; see equation (2.12). The direction of the pressure force vector is perpendicular to the face at which it is applied.

$$M_{pressure} = \sum_{all\ faces} (\mathbf{r} \times \mathbf{F}_{pressure}) \cdot \hat{\mathbf{n}} \quad (2.12)$$

The viscous force is the product between an area and the viscous stresses on that area. The viscous stresses are denoted τ_{ij} , where the index i indicates which surface the stress is applied to and index j indicates which direction the stress is acting. For an incompressible Newtonian fluid, the viscous stresses are approximated by equation (2.13).

$$F_{viscous} = \tau_{ij} dA = \mu \left(\frac{\partial u_i}{\partial x_j} + \frac{\partial u_j}{\partial x_i} \right) dA \quad (2.13)$$

The moment about the fixed axis due to the viscous forces are also calculated by summing the cross product between the viscous forces and the position vector for all faces.

$$M_{viscous} = \sum_{all\ faces} (\mathbf{r} \times \mathbf{F}_{viscous}) \cdot \hat{\mathbf{n}} \quad (2.14)$$

To change the closing time of a tilting disc check valve, an auxiliary spring can be attached to it. The moment exerted on the disc due to the spring can be calculated using equation (2.15), where κ is the torsion coefficient and θ is the angular winding from the equilibrium state. This is an angular version of Hooke's law.

$$M_{spring} = -\kappa\theta \quad (2.15)$$

If all the moments that can act on a tilting disc check valve are inserted into Newton's second law, the resulting equation becomes:

$$I_0\alpha = M_{gravity} + M_{friction} + M_{pressure} + M_{viscous} + M_{spring} \quad (2.16)$$

If the moment of inertia and the moments in equation (2.16) are known, the angular acceleration can be determined. Using the definition of the angular acceleration, seen in equation (2.17), the change in angular velocity, $\Delta\omega$, for a time step, Δt , and the new angular velocity, ω , can then be obtained as in equation (2.18).

$$\alpha = \frac{d\omega}{dt} \rightarrow \alpha dt = d\omega \quad (2.17)$$

$$\Delta\omega = \alpha \Delta t \rightarrow \omega = \omega_{prev} + \alpha \Delta t \quad (2.18)$$

The angular change in every time step is calculated similarly as the change of angular velocity with the definition of the angular velocity as basis; see equation (2.19).

$$\omega = \frac{d\theta}{dt} \rightarrow \omega dt = d\theta \quad (2.19)$$

The new angle in a discrete time step is described in equation (2.20).

$$\theta = \theta_{prev} + \omega \Delta t \quad (2.20)$$

2.3 Computational fluid dynamics

2.3.1 Governing equations of fluid flows

The governing equations for fluid flows are the equations that describe the conservation of mass, momentum, and energy of the fluid. The conservation equation for mass, states that the change of mass of a fluid element should be balanced by the amount of mass flowing through the boundaries of the fluid element. The conservation equation for mass can be seen in equation (2.21).

$$\frac{\partial \rho}{\partial t} + \frac{\partial(\rho u_i)}{\partial x_i} = 0 \quad (2.21)$$

The equation for conservation of momentum, which can be seen in equation (2.22), is based on Newton's second law. In the momentum equation, the rate of change of momentum in a fluid element should be balanced by the rate of momentum transferred through the boundaries of the fluid element and the forces acting on that element. The forces acting on a fluid element is pressure forces, viscous forces, gravitational forces, and possibly additional body forces.

$$\frac{\partial \rho u_i}{\partial t} + \frac{\partial \rho u_i u_j}{\partial x_j} = -\frac{\partial p}{\partial x_i} + \frac{\partial \tau_{ji}}{\partial x_j} + \rho g_i + S_M \quad (2.22)$$

For an incompressible Newtonian fluid, the viscous stresses are described in equation (2.23). Incorporating this into the momentum equation gives the Navier–Stokes equations; see equation (2.24).

$$\tau_{ji} = \mu \left(\frac{\partial u_i}{\partial x_j} + \frac{\partial u_j}{\partial x_i} \right) \quad (2.23)$$

$$\frac{\partial \rho u_i}{\partial t} + \frac{\partial \rho u_i u_j}{\partial x_j} = -\frac{\partial p}{\partial x_i} + \frac{\partial}{\partial x_j} \left[\mu \left(\frac{\partial u_i}{\partial x_j} + \frac{\partial u_j}{\partial x_i} \right) \right] + \rho g_i + S_M \quad (2.24)$$

The derivation of the energy equation is based on the first law of thermodynamics, which states that the change of energy of the fluid element should be equal to the heat transferred into the fluid element and the work done on the fluid element. The energy equation is often written in terms of enthalpy as in equation (2.25). The change in energy of a fluid element is due to work done by pressure forces and viscous forces on the fluid element, due to heat transferred by convection to the fluid element, and due to additional source terms.

$$\frac{\partial(\rho h)}{\partial t} - \frac{\partial p}{\partial t} = -\frac{\partial(\rho h u_j)}{\partial x_j} + \frac{\partial}{\partial x_j} \left(k_n \frac{\partial T}{\partial x_i} \right) + \frac{\partial(\tau_{kj} u_k)}{\partial x_j} + S_h \quad (2.25)$$

If the flow of interest is incompressible and no heat transfer is involved, it is not necessary to solve the energy equation. [5]

2.3.2 Turbulence

Many fluid flows are turbulent. A turbulent flow is characterised by several different features. They are irregular, three-dimensional, and dissipative. They occur at high Reynolds numbers, they can be treated like a continuum, and the diffusivity increases when the flow becomes turbulent. [6]

In a turbulent flow, there exist a whole spectrum of different velocity, length, and time scales. The largest scales extract their kinetic energy from the mean flow while the smaller scales extract their kinetic energy from the somewhat larger scales. Most of the kinetic energy is then dissipated to internal energy by viscous forces at the smallest scales. The size of the largest scales is restricted by the flow geometry while the size of the smallest scales is restricted by the viscosity. When studying a fluid, the smallest scales in a turbulent flow are larger than the size of the molecules and the flow can be treated as a continuum. The rotational motion of the turbulent scales are called eddies and the presence of eddies in the flow generates irregular fluctuations of the flow variables. [7]

The motion of eddies also increases the diffusivity of a turbulent flow. This means that the exchange of mass, momentum, and heat increases when the flow becomes turbulent. To get an indication if the flow is turbulent, the Reynolds number can be calculated. When the Reynolds number is high enough, the flow will become turbulent and the inertial forces will then dominate. At low Reynolds number, the flow is laminar and the viscous forces are dominant. The Reynolds number for a pipe flow can be calculated using equation (2.26), where U is the mean velocity of the flow, L is the hydraulic diameter of the pipe, and ν is the kinematic viscosity. [5]

$$Re = \frac{UL}{\nu} \quad (2.26)$$

2.3.3 Turbulence modelling

To resolve all the time and length scales in a turbulent flow during a simulation requires a fine resolution in both time and space. In direct numerical simulations, the Navier–Stokes equations are solved directly, which means that the spatial and temporal resolution has to be

fine. This requires large computational resources, which today makes it necessary to use other approaches for most turbulent flows.

The instantaneous flow variables in a turbulent flow consist of a mean value and a fluctuating part. Instead of resolving all the time and length scales, the instantaneous flow variables, φ , can be decomposed into the mean, ϕ , and the fluctuating part, φ' , as seen in equation (2.27).

$$\varphi = \phi + \varphi' \quad (2.27)$$

The mean of a flow variable is the time averaged value of that flow variable and it is written as:

$$\phi = \frac{1}{\Delta t} \int_t^{t+\Delta t} \varphi dt \quad (2.28)$$

The time interval, Δt , for which the flow variables are averaged, should be larger than the time scales of the turbulent fluctuations, but smaller than the time scales of the variations in the mean values of the flow properties. [5] [8] The flow variables, which are decomposed when an incompressible fluid without any heat transfer is studied, are the pressure and the velocities, i.e.:

$$u_i = U_i + u'_i \quad (2.29)$$

$$p = P + p' \quad (2.30)$$

To obtain the conservation equations for the mean values of the flow properties, the decomposed flow properties are inserted into the continuity equation and the Navier–Stokes equation. The new equations are then averaged over time. The time averaged conservation equations can be seen in equation (2.31) and equation (2.32), where the gravitational forces and other body forces has been neglected and an incompressible fluid has been assumed. [5]

$$\overline{\frac{\partial \rho(U_i + u'_i)}{\partial x_i}} = 0 \quad (2.31)$$

$$\begin{aligned} \overline{\frac{\partial \rho(U_i + u'_i)}{\partial t}} + \overline{\frac{\partial \rho(U_i + u'_i)(U_j + u'_j)}{\partial x_j}} \\ = -\frac{\partial(P + p')}{\partial x_i} + \frac{\partial}{\partial x_j} \left[\mu \left(\frac{\partial(U_i + u'_i)}{\partial x_j} + \frac{\partial(U_j + u'_j)}{\partial x_i} \right) \right] \end{aligned} \quad (2.32)$$

The time average of an already time averaged value is still the same value, while the time average of a random fluctuating component is zero. If these relations are used on equation (2.31) and equation (2.32) and the terms are rearranged, the equations reduce to equation (2.33) and equation (2.34). These equations are called the Reynolds-averaged Navier–Stokes equations. [5]

$$\frac{\partial(\rho U_i)}{\partial x_i} = 0 \quad (2.33)$$

$$\frac{\partial \rho U_i}{\partial t} + \frac{\partial \rho U_i U_j}{\partial x_j} = -\frac{\partial P}{\partial x_i} + \frac{\partial}{\partial x_j} \left[\mu \left(\frac{\partial U_i}{\partial x_j} + \frac{\partial U_j}{\partial x_i} \right) - \rho \overline{u'_i u'_j} \right] \quad (2.34)$$

The extra terms, $-\rho \overline{u'_i u'_j}$, which appear in the Navier–Stokes equations after the time averaging, are called the Reynolds stresses. The Reynolds stresses appears due to turbulent momentum transfer. To close the Reynolds-averaged Navier–Stokes equations, these terms have to be modelled. [5]

To model the Reynolds stress tensor, two different approaches are often used: the eddy viscosity turbulence model and the Reynolds stress model. In the eddy viscosity turbulence models, either an algebraic equation or one or two additional transport equations is solved, while in the Reynolds stress model seven additional transport equations are used. The extra seven equations makes it more computational expensive than the eddy viscosity turbulence models and the eddy viscosity turbulence models will therefore be considered in this thesis.

2.3.4 Eddy viscosity turbulence models

In the eddy viscosity turbulence models, the Boussinesq assumption is used to get an expression for the Reynolds stress tensor. In the Boussinesq assumption, the Reynolds stresses are set to be proportional to the gradients of the mean velocities, where the dynamic turbulent viscosity, μ_t , are the variable of proportionality. To make the relation valid upon contraction, an additional term, which includes the turbulent kinetic energy, has to be added. [6] The Boussinesq assumption can be seen in equation (2.35), where the turbulent kinetic energy is given by equation (2.36).

$$\rho \overline{u'_i u'_j} = -\mu_t \left(\frac{\partial U_i}{\partial x_j} + \frac{\partial U_j}{\partial x_i} \right) + \frac{2}{3} \delta_{ij} \rho k \quad (2.35)$$

$$k = \frac{1}{2} \overline{u_i u_i} \quad (2.36)$$

The Boussinesq assumption introduces the approximation that the turbulence is isotropic, which is a disadvantage, in comparison to large eddy simulation or direct numerical simulations. [7]

To solve the Reynolds-averaged Navier–Stokes equations, the unknowns in equation (2.35) have to be determined. To obtain an expression for the dynamic turbulent viscosity, dimensional analysis is performed. The dynamic turbulent viscosity can be expressed in terms of the kinematic turbulent viscosity, ν_t , i.e. $\mu_t = \rho \nu_t$. The kinematic turbulent viscosity has the dimension m^2/s . To get the right dimension for the kinematic turbulent viscosity, a velocity scale and a length scale can be used. The velocity scale, ϑ , and the length scale, ℓ , for the largest turbulent scales are used, because most of the turbulent transport is performed by these scales. The resulting expression for the dynamic turbulent viscosity can be seen in equation (2.37). [6]

$$\mu_t = \rho\nu_t = \rho C\vartheta\ell \quad (2.37)$$

In the algebraic models, the turbulent viscosity is calculated using an algebraic equation. The algebraic equations require the least computational resources of the eddy viscosity turbulence models, but it is the model that performs the worst when modelling the turbulence. The algebraic model does not take the transport of turbulent properties into account and the model has to be calibrated to the specific flow. [6] [7] [8]

In one-equation models, one extra transport equation is solved. The turbulent quantity, which is modelled by this extra transport equation, is often the turbulent kinetic energy. The turbulent quantity determined from the extra transport equation can be used to determine one of the turbulent scales in equation (2.37). However, the other scale still has to be determined using an algebraic equation. [7]

If two turbulent quantities are modelled, each using its own transport equation, then both the turbulent length scale and the turbulent velocity scale can be determined from these quantities. This is what is done in the two-equation models. The most common set of turbulent properties that are modelled in the two transport equations are the turbulent kinetic energy together with either the dissipation rate, ε , or the specific dissipation rate, ω .

The exact equation for the turbulent kinetic energy is derived by first subtracting the Reynolds-averaged Navier–Stokes equations from the Navier–Stokes equation. The result is multiplied with the fluctuating velocity component and it is then time averaged. The resulting equation consists of four unknown terms that has to be modelled in order to close the equation. [5]

The modelled k – equation can be seen in equation (2.38), where the terms on the left hand side represents the rate of change of k and convective transport of k respectively. The first term on the right hand side represents diffusive transport of k , while the two last terms describe the production and dissipation of k . The terms for production, dissipation and turbulent diffusion of k are the terms that have been modelled to close the k – equation. [5]

$$\frac{\partial \rho k}{\partial t} + \frac{\partial \rho U_j k}{\partial x_j} = \frac{\partial}{\partial x_j} \left[\left(\mu + \frac{\mu_t}{\sigma_k} \right) \frac{\partial k}{\partial x_j} \right] + \mu_t \left(\frac{\partial U_i}{\partial x_j} + \frac{\partial U_j}{\partial x_i} \right) \frac{\partial U_i}{\partial x_j} - \rho \varepsilon \quad (2.38)$$

2.3.4.1 The k – ε model

In the k – ε models, the second transport equation is solved for the dissipation rate. The exact ε – equation also contains unknown terms, which are modelled in order to solve the system of equations. The modelled ε – equation can be seen in equation (2.39), where the terms on the left hand side are the rate of change and convection of ε respectively. The terms on the right hand side are the diffusion of ε , production of ε and destruction of ε respectively. [5]

$$\frac{\partial \rho \varepsilon}{\partial t} + \frac{\partial \rho U_j \varepsilon}{\partial x_j} = \frac{\partial}{\partial x_j} \left[\left(\mu + \frac{\mu_t}{\sigma_\varepsilon} \right) \frac{\partial \varepsilon}{\partial x_j} \right] + c_{\varepsilon 1} \mu_t \frac{\varepsilon}{k} \left(\frac{\partial U_i}{\partial x_j} + \frac{\partial U_j}{\partial x_i} \right) \frac{\partial U_i}{\partial x_j} - c_{\varepsilon 2} \rho \frac{\varepsilon^2}{k} \quad (2.39)$$

Using k and ε to determine the dynamic turbulent viscosity, dimensional analysis yields the expression for the dynamic turbulent viscosity seen in equation (2.40). The constants σ_k , σ_ε , $c_{\varepsilon 1}$, $c_{\varepsilon 2}$ and c_μ in the equations for k , ε and μ_t have previously been determined to agree as good as possible with the result from several experimental flows. These constants can however be adjusted to fit specific experiments.

$$\mu_t = \rho c_\mu \frac{k^2}{\varepsilon} \quad (2.40)$$

The $k - \varepsilon$ model described above is called the standard $k - \varepsilon$ model. The standard $k - \varepsilon$ model works best for high Reynolds number flows, for which it is designed. The standard $k - \varepsilon$ model performs poor in predicting the turbulent normal stresses and in flows with adverse pressure gradients. Other disadvantages with the standard $k - \varepsilon$ model are that it performs poor for flows involving swirling motion, curved boundary layers, and separation. [5] [7] [9]

There are also other $k - \varepsilon$ models available. One of them is the realizable $k - \varepsilon$ model. In the realizable $k - \varepsilon$ model, the constant in the equation for the turbulent viscosity, c_μ , has been modified. This is done to fulfil Schwarz inequality for the shear stresses and to always obtain a positive value of the normal components of the Reynolds stresses. Instead of using a constant value of c_μ , a variable value is used. Otherwise, the same equation is used to calculate the turbulent viscosity. [9]

The equation for the dissipation rate is also different from the standard $k - \varepsilon$ model. The terms for production and destruction of ε have been modified, as can be seen in equation (2.41). This modification removes the singularity problem, which can occur for the destruction term in the standard $k - \varepsilon$ model when k approaches zero. The constants in the $k -$ equation and in the $\varepsilon -$ equation are changed to give a good result for the new transport equations. [9]

$$\frac{\partial \rho \varepsilon}{\partial t} + \frac{\partial \rho U_j \varepsilon}{\partial x_j} = \frac{\partial}{\partial x_j} \left[\left(\mu + \frac{\mu_t}{\sigma_\varepsilon} \right) \frac{\partial \varepsilon}{\partial x_j} \right] + \rho c_{\varepsilon 1} \varepsilon \sqrt{2S_{ij}S_{ij}} - c_{\varepsilon 2} \rho \frac{\varepsilon^2}{k + \sqrt{\frac{\mu}{\rho}} \varepsilon} \quad (2.41)$$

$$c_{\varepsilon 1} = \max \left[0.43, \frac{\eta}{\eta + 5} \right] \quad (2.42)$$

$$\eta = \sqrt{2S_{ij}S_{ij}} \frac{k}{\varepsilon} \quad (2.43)$$

The realizable $k - \varepsilon$ model is more appropriate for use in flows with high strain rates, than the standard $k - \varepsilon$ model due to the introduced changes. The realizable $k - \varepsilon$ model has shown better performance than the standard $k - \varepsilon$ model in flows involving swirl, separation, rotation, and boundary layers. It has also shown better performance in flows with strong streamline curvature. It is, however, not as stable as the standard $k - \varepsilon$ model. [7] [9]

2.3.4.2 The $k - \omega$ model

The $k - \omega$ model is also widely used. It handles the flow near the wall better than the $k - \varepsilon$ models. However, it requires a finer mesh close to the wall. The transport equations and the turbulent viscosity for the model can be seen in equation (2.44), equation (2.45) and equation (2.46).

$$\frac{\partial \rho k}{\partial t} + \frac{\partial \rho U_j k}{\partial x_j} = \frac{\partial}{\partial x_j} \left[\left(\mu + \frac{\mu_t}{\sigma_k^\omega} \right) \frac{\partial k}{\partial x_j} \right] + \mu_t \left(\frac{\partial U_i}{\partial x_j} + \frac{\partial U_j}{\partial x_i} \right) \frac{\partial U_i}{\partial x_j} - \rho \beta^* \omega k \quad (2.44)$$

$$\frac{\partial \rho \omega}{\partial t} + \frac{\partial \rho U_j \omega}{\partial x_j} = \frac{\partial}{\partial x_j} \left[\left(\mu + \frac{\mu_t}{\sigma_\omega} \right) \frac{\partial \omega}{\partial x_j} \right] + c_{\omega 1} \mu_t \frac{\omega}{k} \left(\frac{\partial U_i}{\partial x_j} + \frac{\partial U_j}{\partial x_i} \right) \frac{\partial U_i}{\partial x_j} - \rho c_{\omega 2} \omega k \quad (2.45)$$

$$\mu_t = \rho \frac{k}{\omega} \quad (2.46)$$

2.3.5 Near wall modelling

Close to a solid boundary the solution variables changes rapidly. This boundary layer is divided into two regions, the outer region, and the inner region where the treatment of the inner region is of primary interest. The inner region consist of the viscous sub-layer, where the viscous stresses are dominant, of the buffer layer, where the viscous and Reynolds stresses are of similar size, and of the fully turbulent layer, where the Reynolds stresses are dominant. [10] To give an indication of the extent of the different regions a dimensionless length, y^+ , is used.

There are different ways to model the flow in the inner region. When using wall functions to model the near wall region, the viscous sub-layer and the buffer layer are not resolved. Instead, the first grid point is placed in the fully turbulent layer, $30 < y^+ < 100$. [7] This approach does not require a fine near wall mesh, but values of $y^+ < 30$ should be avoided because this could cause an incorrect prediction of the wall shear stresses. [9]

In the low-Reynolds-number turbulence model, the flow is also resolved in the near wall region. For turbulence models, which are invalid in this region, a modification of the equations has to be done in order to make them valid in the near wall region. Dampening functions are often used to modify the invalid equations. The low-Reynolds-number turbulence models requires a fine near wall mesh with the first grid point at an y^+ – value of approximately 1. [7]

In ANSYS Fluent, enhanced wall treatment can also be used to model the near wall region. In the enhanced wall treatment, a two-layer zonal model is used if the mesh in the near wall region is fine enough. If the mesh is coarse close to the wall and if the use of wall functions is preferable, enhanced wall functions are used instead. This makes the enhanced wall treatment less sensitive to which y^+ – value that is used in the first grid point. [10]

2.3.6 Boundary conditions

To solve a CFD problem, appropriate boundary conditions needs to be specified. For a problem involving pipe flow with incompressible water, one has to specify the boundary

conditions for the inlet, the outlet, and the walls. There are different ways to specify these boundary conditions. For the inlet, a pressure, velocity, or mass flow boundary condition can be used while for the outlet, a pressure or outflow boundary condition can be used. At the walls, the no-slip boundary condition is usually used for the velocity components. [7]

If a turbulent flow is considered, the boundary conditions for the turbulent properties must be given. If the turbulent properties modelled are not known at the boundaries, other appropriate turbulent properties can be used to specify the boundary condition. For a pipe flow, the turbulent intensity and hydraulic diameter can be used. The turbulent intensity in a pipe flow can be calculated using equation (2.47), where the Reynolds number is given by equation (2.26). [9]

$$I_t = 0.16Re^{-1/8} \quad (2.47)$$

The profile of the flow variables should be specified at the boundaries. If these are not known, an average value can be used. If an average value is used, the inlet and outlet should be placed far from the investigated part. [7] This is to ensure that a fully developed flow is obtained before reaching the part of interest.

2.3.7 Discretisation schemes

In order to calculate the flow, the flow domain has to be discretized in both space and time.

2.3.7.1 Spatial discretization

In computational fluid dynamics, the governing equations can be discretized using a control volume approach. The fluid domain is then divided into cells, over which the transport equations are integrated. In the integrated equations, the solution variables in the convection term and the gradient of the solution variables in the diffusion term are given at the faces of the cell. The value of the solution variables are however calculated in the centre of each cell. In the diffusion term, central differencing is used to estimate the gradient of the solution variables at the faces of the cells, using the values from the cell centre. For the convective term, several different discretization schemes exist to calculate the face values of the solution variables from the node values. [10]

Some of these discretization schemes for the convective term, which also are available in the ANSYS Fluent are the first order upwind scheme, the second order upwind scheme, the power law scheme, the Quadratic Upstream Interpolation for Convective Kinetics scheme (QUICK scheme), and the third order Monotone Upstream-centred Schemes for Conservation Laws (MUSCL scheme). [7] [10]

When assigning values to the faces of the cells, the first order upwind scheme uses the upstream cell centre value. This is done in order to account for the direction of the flow. The first order upwind scheme is only first order accurate but it is bounded. [5] A drawback of a first order accurate scheme is that the numerical diffusion is higher than for discretization schemes of higher accuracy. [9]

In the second order upwind scheme, the face values are determined by equalizing the derivative between the two upstream cell centres from the face, and the derivative between the

face and the first upstream cell centre. The second order upwind scheme is second order accurate, and it is good for both convective and diffusive flows but it is unbounded. [7]

When the power law scheme is used to determine the face values, a one-dimensional convection diffusion equation is solved using the cell centre values of the two neighbouring cells. [5] [7] [10] The power law scheme works best for flows where the Peclet number, i.e. the ratio between the rate of convection and the rate of diffusion, is below 10. [7]

In the QUICK scheme three different cell centre values are used to estimate each face value, the two nearest upstream and the downstream cell centre values. The face value is then determined by adapting a quadratic function through the three cell centre values. [5] The QUICK scheme is third order accurate and it works well for both convective and diffusive flows. It is an unbounded scheme and in ANSYS Fluent it is only used for hexahedral or quadrilateral meshes. [7] [10]

The third order MUSCL scheme uses a mixture of the second order upwind scheme and the central differencing scheme in order to calculate the values at the cell faces. [10] The spatial accuracy for swirling and rotating flows can be improved by using the third order MUSCL scheme instead of the second order upwind scheme. [7]

2.3.7.2 Temporal discretization

If the flow condition is transient, a time-discretization is applied to the transport equations. For the terms in the transport equations, integration is performed over a time step. The implicit time integration, the bounded second order implicit time integration, and the explicit time integration are temporal discretization methods in ANSYS Fluent. [10]

The implicit time integration method in ANSYS Fluent is a fully implicit scheme that uses the future values of the flow variables for all terms in the equations except for the accumulation term. In the accumulation term both the new and old value of the flow variables appear. Because the future value is used in the equations, a number of iterations are required in each time step to reach convergence. One advantage of the implicit scheme is that any time step size can be used, since it is unconditionally stable. However, the implicit scheme is only first order accurate and therefore a small time step size should be used in order to obtain an accurate solution. [5] [10]

The bounded second order implicit time integration method uses both the new and the old values of the flow variables for all terms in the equations. Hence, iterations are required to obtain a converged solution. In ANSYS Fluent, this method is not available for meshes where deformation or motion occurs. [10]

In the explicit time integration method, the old values are used for all terms except the accumulation term. Because the old value is used, no iterations are required within each time step. In this method, the time step should be chosen to fulfil the Courant–Friedrichs–Lewy (CFL) condition seen in equation (2.48). [5] [7] [10]

$$\Delta t < CFL \min \left(\frac{\rho(\Delta x)^2}{\Gamma}, \frac{\Delta x}{U} \right) \quad (2.48)$$

If the condition in equation (2.48) is not fulfilled, the solution often diverges, but if it converges, the simulation with the explicit scheme is faster than the simulation with the implicit schemes. [7]

2.3.8 Choosing the pressure-velocity coupling algorithm

In ANSYS Fluent, there are two different algorithms for the pressure-based solver. Either a pressure-based coupled algorithm or a pressure-based segregated algorithm can be used. In the segregated algorithm, the solution variables are updated separately in each iteration. In the coupled algorithm however, the momentum equations and pressure-based continuity equation is solved simultaneously in each iteration, while the other equations are updated separately. The required memory capacity will therefore be larger for the coupled algorithm than for the segregated algorithm, because the number of discretized equations that needs to be stored at the same time is larger for the coupled algorithm. The advantage of the coupled algorithm compared to the segregated algorithm is that it converges faster. [10]

2.4 Meshing

ANSYS Fluent can handle several types of meshes. In two-dimensional simulations, triangular or quadrilateral cells can be used and in three-dimensions, tetrahedral, wedge/prism, hexahedral, pyramid, and polyhedral cells can be used. The mesh can be constructed by a combination of the different types of cells. Depending on the applications, different types of meshes are more favourable. In order to select cell types for a certain problem, three factors should be considered: the setup time, the computational expense, and the numerical diffusion. If the geometry is complex, the use of a structured mesh may be computational expensive. Using a structured mesh can result in poor quality of the mesh. It can also lead to simplifying the problem too much, but it might also be the other way around; the mesh might have an unnecessarily high number of cells in unimportant areas.

When it comes to the computational expense, the use of quadrilateral or hexahedral cells is preferable in comparison with the triangular or tetrahedral cells. The advantage is due to the fact that the aspect ratio is allowed to be larger for the quadrilateral or hexahedral cells. For a triangular or tetrahedral mesh, a large aspect ratio always leads to skewness, which in turn can cause convergence and accuracy problems. The number of elements is often lower for meshes consisting of triangular or tetrahedral cells when there is a complex geometry, but for a simple geometry, the use of quadrilateral or hexahedral cells results in fewer cells. Numerical diffusion has the greatest impact on the results when the real physical diffusion is low and when the convection is large. The numerical diffusion is smaller when the flow is mesh-oriented, and when the mesh has better resolution, the numerical diffusion influence is better. [9] A structured mesh is thus preferable because of the better numerical properties but cannot always be applied for complex geometries.

The mesh has a large impact on the solution and in order to get an acceptable mesh the quality must be verified. A high quality mesh is important in order to get adequate accuracy and

stability of the calculation. To verify the quality of the mesh the orthogonal quality, the aspect ratio, and the skewness of the cells can be examined. The mesh quality is assumed acceptable when the orthogonal quality is larger than 0.01 and the aspect ratio and skewness are lower than 10 and 0.95 respectively. [7] [9]

2.4.1 Dynamic mesh

Three different methods can be used to update the mesh when the boundary changes. Those methods are the smoothing methods, the dynamic layering, and the remeshing methods. The three methods can be used separately or in combination with each other, depending on the current mesh motion. The methods are described in the three following subchapters. [9]

2.4.1.1 Smoothing methods

This method applies smoothing to the mesh when it changes in every time step. The change occurs at a boundary and it can be a movement or a deformation of the boundary. The smoothing affects the mesh, but the amount of nodes and edges are constant and the joints between the cells are still the same.

One of the smoothing methods is the spring-based smoothing method. In the spring-based smoothing method, the edges in the mesh are described as springs. One node has at least two edges connected to it, i.e. two springs. The structure of the mesh before starting a calculation is said to be the equilibrium state. When the boundary moves, the springs will be displaced. The new location for the nodes will be at a position so that every node is in equilibrium due to the forces from the springs. The spring-based smoothing method is mainly used for tetrahedral or triangular meshing cells.

Another smoothing method is the diffusion-based smoothing. In the diffusion-based smoothing method, the diffusion equation, seen in equation (2.49), is used to update the new position of the elements in the mesh. The diffusion coefficient can either be expressed in terms of the distance from the moving boundary or the cell volume. [9]

$$\nabla \cdot (\gamma \nabla \mathbf{u}) = 0 \quad (2.49)$$

2.4.1.2 Dynamic layering

Dynamic layering is a method in which cells can be created or deleted when a boundary of the mesh moves. If new cells shall occur, the mesh must be extruded in that area and if cells shall vanish, the mesh must be compressed in that area. When a cell is added to the mesh, there is actually a split of an existing cell near the boundary. The threshold for the cell splitting is the distance between the boundary and the next cell. The method is equivalent for the removal of a cell, but instead of splitting a cell, the two cells closest to the boundary are merged together when the threshold is reached. The dynamic layering can be applied to hexahedral or wedge cells. [9]

2.4.1.3 Remeshing methods

If the movement of the boundary is large in comparison with the cell size, problems might occur. For example, the volume of a cell may become negative, which leads to convergence issues. ANSYS Fluent has methods to prevent those problems, e.g. by updating the mesh in

the next time step. Different methods are applicable on different types of cells. For example in three-dimensions, tetrahedral cells must be used when the local cell and local face remeshing methods are applied. The local cell and face remeshing method is often used in the first case and it can be applied on cells and faces respectively. If the local remeshing method is not sufficient, the zone remeshing method is used. The zone remeshing method has a stricter requirement for when the mesh needs to be remeshed. The number of cells changes every time the mesh is remeshed. The frequency of the remeshing depends on the settings in ANSYS Fluent, e.g. the skewness, minimum, and maximum length. [9]

2.5 User-defined functions

A UDF is a method that can be used to make ANSYS Fluent perform specific actions that is not included in the tool itself. In order to integrate with ANSYS Fluent, the UDF, which is written in the program language C, has to be created according to a specific pattern. Each UDF has to contain specific DEFINE macros created for ANSYS Fluent. ANSYS Fluent also supplies other macros and predefined functions that can be used to interact with the tool. The UDFs can be used, for example, to describe the movement of a body or to control a boundary condition in a specific way. Other applications are, to control the time step size automatically and to write data to a file in every time step or iteration. [11]

3 Input conditions of the CFD simulation

The setup of the experiment, on which this master's thesis is based, will be two tanks working as water supplies for the piping system. One of the tanks will have a higher pressure, which will force the water to flow to the other tank. However, a pump will be installed in the system that forces the water to flow in the opposite direction. Downstream the pump, a horizontally installed check valve will be located. This check valve can be switched and either a tilting disc check valve or a swing check valve will be used. As long as the pump is operating and the flow is sufficient, the check valve will be open. In the experiment, the pump will be shut down in order to reconstruct the situation of a pump trip. As the pump is tripped, the flow will decrease and hence induce closing of the check valve. The dynamic characteristic of the check valve will then be studied during this transient. In the following subchapters, the geometry and the properties of the tilting disc check valve, the properties of the fluid, and the boundary conditions, are presented.

3.1 Geometry of the tilting disc check valve

The tilting disc check valve that will be studied in the experiment is investigated in this master's thesis. The design of the interior of the tilting disc check valve can be seen in Figure 2. A CAD model of the valve is created using two-dimensional drawings, illustrating cross sections of the check valve; see example in Figure 3. The CAD model is provided by OKG and ÅF and imported to ANSYS DesignModeler, where the geometry is adjusted in order to make it appropriate for a CFD simulation. As boundary conditions to the valve housing, the inlet and outlet pipes are extended and assumed straight with a length of 5 m respectively. A fluid domain is then produced using the bounding surfaces from the CAD model and the pipes. In order to perform a CFD analysis, the fluid domain is later divided into cells forming a computational mesh; see chapter 4.2.1. Outside the fluid domain, a lever arm with a removable weight is located and attached to the check valve disc via the rotating axis.

The coordinates of the geometry is oriented in the following way; the x – axis is located in the flow direction, the y – axis is oriented upwards, and the z – axis is located along the rotational axis. When the disc is fully open, the angle is 65 degrees and when the disc is fully closed the angle is 0 degrees. The angular velocity is negative when the disc closes.

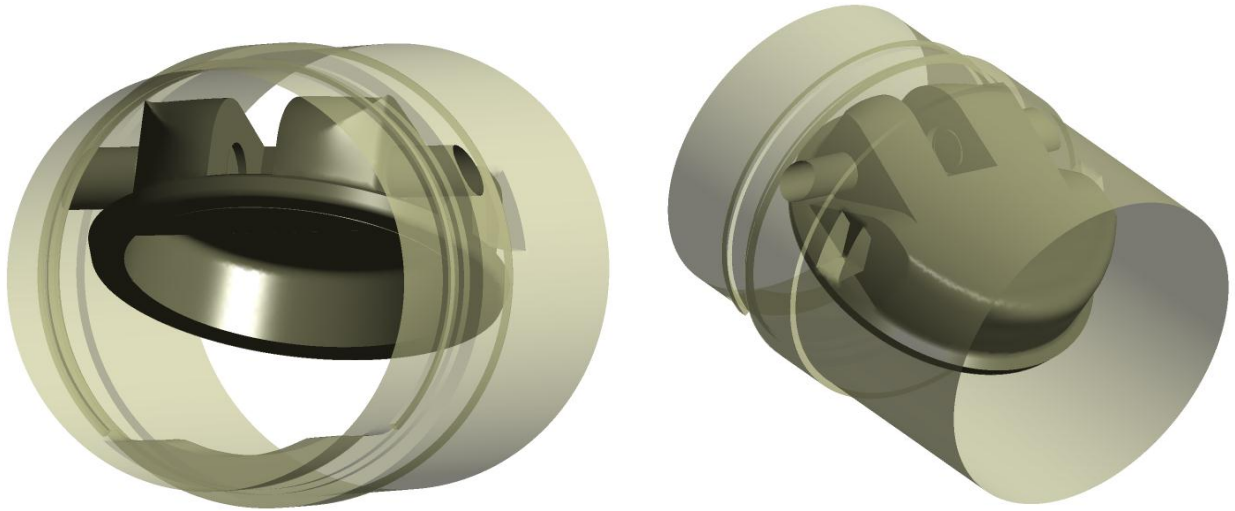


Figure 2: The geometry of the interior of the tilting disc check valve. The left figure shows the check valve from the front while the right figure shows the check valve from the back. Note the differences of the arms.

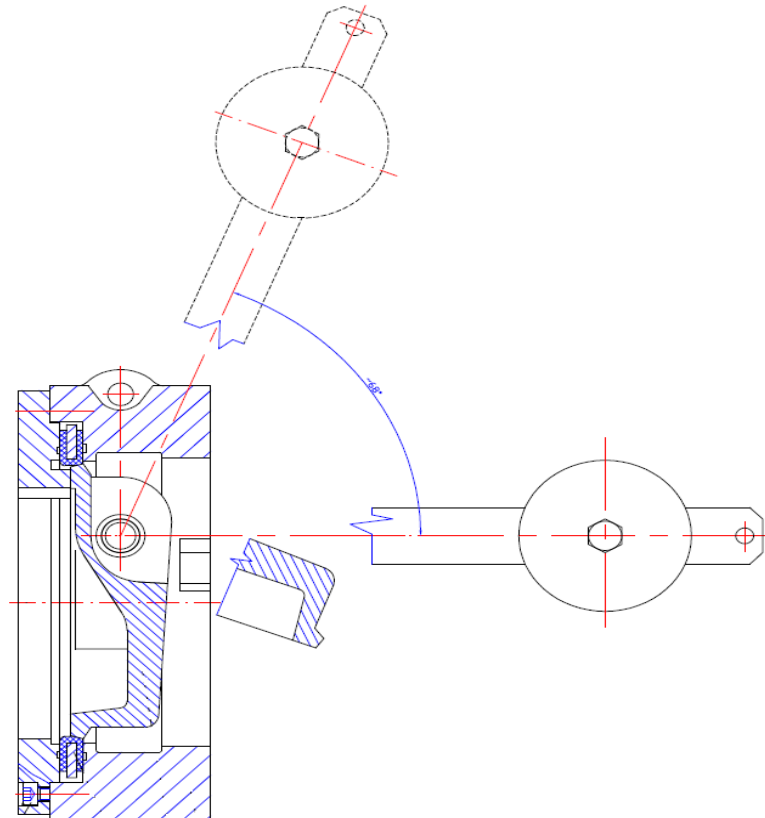


Figure 3: A cross-section of the tilting disc check valve in the $x - y$ plane.

3.2 Properties of the tilting disc check valve

The important properties of the check valve are the mass, the centre of mass, and the moment of inertia of the different rotating parts. The check valve is divided into 3 parts: the disc, the arm, and the removable weight. The arm is in turn consisting of four parts for which the total mass, the centre of mass, and the moment of inertia are calculated and added together. The

centre of mass of the composed arm is calculated according to equation (2.6). The total mass, the centre of mass, and the moment of inertia of the three parts can be seen in Table 1.

The disc has a complex geometry and an analytic solution of the moment of inertia and the centre of mass of the disc are therefore hard to calculate. Instead, the moment of inertia is calculated in the CAD-program SolidWorks and the mass centre is calculated in ANSYS DesignModeler.

To calculate the moment of inertia for the arm and the removable weight, different standard expressions of the moment of inertia are used. The parallel axis theorem, defined in equation (2.3), is applied to obtain the moment of inertia about the right axis and the superposition principle is applied to obtain one value for the moment of inertia of the arm. The moments of inertia, used to describe the different parts of the arm and of the removable weight are: a point mass, a solid cylinder, a thick-walled cylindrical tube, and a solid cuboid.

Table 1: Mass, centre of mass, and moment of inertia for the disc, arm, and removable weight.

Total mass of different parts	Centre of mass relative the z-axis	Moment of inertia around the z-axis
$m_{disc} = 1.397 \text{ kg}$	$cm_{disc} = 0.0297 \text{ m}$	$I_{disc} = 0.00270 \text{ kg m}^2$
$m_{arm} = 0.883 \text{ kg}$	$cm_{arm} = 0.0689 \text{ m}$	$I_{arm} = 0.0100 \text{ kg m}^2$
$m_{weight} = 1.018 \text{ kg}$	$cm_{weight} = 0.243 \text{ m}$	$I_{weight} = 0.0601 \text{ kg m}^2$

3.3 Properties of the fluid

The fluid in the experiment will be water at room temperature. Therefore, the fluid in the simulations are assumed to be incompressible water at 20 °C. The density of water at 20 °C is 998.2 kg/m³ and the dynamic viscosity is 0.001003 kg/(m · s). [12]

3.4 Boundary conditions

The inlet and outlet boundaries are placed 5 m away from the check valve, i.e. the pipes are extended with 5 m. This is done in order to obtain a fully developed turbulent flow at the check valve.

3.4.1 Inlet boundary condition

The inlet boundary condition is chosen to be a mass flow inlet. The mass flow rate at normal operating condition will be 30 – 40 kg/s in the experiment. [13] Therefore, the mass flow rate is set to 35 kg/s in the simulations. When the pump trips, the mass flow rate through the inlet starts to decrease. This decrease of mass flow is approximated from studying a pump curve provided by OKG showing the mass flow rate out from the pump after the pump has tripped. The function for the approximation of the mass flow rate is written in equation (3.1).

$$\dot{m} = \frac{35}{140} (-501.69t^3 + 823.76t^2 - 464.13t + 140) \frac{\text{kg}}{\text{s}} \quad (3.1)$$

3.4.2 Outlet boundary condition

At the outlet, a pressure boundary condition is used. The operating pressure in the system is set to 101.3 kPa while the gauge pressure on the outlet is set to 0 Pa.

3.4.3 Boundary condition for the turbulent quantities

The hydraulic diameter and the turbulent intensity are used as boundary conditions for the turbulent quantities at the inlet and outlet of the system. The hydraulic diameter of the pipe at the inlet of the check valve is set to $L_{inlet} = 0.121$ m while the hydraulic diameter at the outlet is set to $L_{outlet} = 0.128$ m. To calculate the turbulent intensity, the average velocities at the inlet and outlet need to be determined. The average velocity is calculated by dividing the mass flow rate by the density and flow area. Inserting the calculated velocities into equation (2.26) give the Reynolds numbers. The Reynolds numbers is in turn used to calculate the turbulent intensities as in equation (2.47). The resulting values for the average velocity, Reynolds number, and turbulent intensity at the inlet and outlet can be seen in Table 2.

Table 2: The average velocity, Reynolds number, and turbulent intensity at the inlet and outlet.

	$U_{average}$	Re	I_t
Inlet	3.05 m/s	$3.68 \cdot 10^5$	3.2 %
Outlet	2.72 m/s	$3.47 \cdot 10^5$	3.2 %

4 Method and application

The outline of this master's thesis was to start with a theoretical study. After the CAD model was received, a two-dimensional case was planned for and performed in order to try different settings, get a working remeshing process and develop and troubleshoot the UDF. The three-dimensional case was there after undertaken where a main analysis was performed. The main analysis consisted of a simulation with the removable weight, hereafter referred to the default simulation, and a simulation without the removable weight. In addition to the main analysis, sensitivity analyses of the default simulation were performed in order to ensure the suitability of the default simulation. Parameters for the mesh and settings for the CFD simulations are explained throughout the following chapters.

4.1 Motion of the tilting disc check valve in a fluid

The angular motion of the tilting disc check valve is determined as described in section 2.2.1. The forces acting on the disc in the experimental setup are gravitational forces, frictional forces, pressure forces, and viscous forces. The frictional forces are unknown, and assumed small in comparison to the other acting forces. Consequently, the frictional forces are neglected in this master's thesis. The equation used to calculate the angular acceleration thus reduced to:

$$\alpha = (M_{gravity} + M_{pressure} + M_{viscous})/I_0 \quad (4.1)$$

The pressure forces and viscous forces are obtained from the calculation of the flow, while the gravitational forces are obtained from the current position of the disc. To solve equation (4.1) several properties of the check valve had to be known; see chapter 3.2. If the angular velocity of the disc is positive, the disc will open and vice versa. A positive net moment will therefore influence the disc to open.

4.2 Main analysis

The main analysis of this master's thesis is to investigate the dynamic characteristics of the tilting disc check valve in order to determine its closing time. The main analysis of the tilting disc check valve includes two simulations, one with and one without the removable weight on the lever arm for correspondence to the experiment. The simulation with the removable weight is the default simulation. Whether or not to include the removable weight is controlled in the UDF. In the UDF, the movement of the disc is determined by the forces from the surrounding fluid and by the gravitational forces. Before the desired transient simulation starts, the UDF representing the investigated case is hooked in ANSYS Fluent version 14.5. The hooking of the UDF is done in order to pass information between the UDF and ANSYS Fluent.

4.2.1 Mesh

The mesh used in the CFD simulations is created using ANSYS Meshing. The fluid domain is divided into different regions, in order to apply different meshing methods. A cross section of the mesh used in the main simulations can be seen in Figure 4, where the different regions are numbered from 1 to 6.

In the fluid domain around the disc, region 3, a tetrahedral mesh is used since the local cell remeshing method requires it. The geometry is complex. A mesh consisting of tetrahedral cells is therefore more likely to give a lower number of cells in this domain compared to a mesh consisting of hexahedral cells. The size of the cells in region 3 is approximately equal, except close to the solid boundaries where the cells are refined. A finer mesh is set at the outer walls of the valve housing in order to obtain a better resolution close to the wall, where the gradients are high. An inflation layer of 1 cell is used at the disc to maintain a good resolution when the disc moves. The thickness of the inflation layer around the disc has to be kept thin, since this cell layer is not remeshed. Consequently, the prism layer thickness is a limitation of the mesh, especially when small gaps between the disc and the valve housing arise, as the valve approaches fully closed. A close-up view of the mesh around the disc can be seen in Figure 5.

In region 1 and 6, a structured hex dominant mesh is used. In these regions, the geometry is simple and the hexahedral mesh applied uses fewer cells than a tetrahedral mesh would do. The largest gradients of the flow variables are close to the solid boundaries and close to the disc. Therefore, the sizes of the cells are chosen to be smallest here. In region 1 and 6, the gradients are not as large as close to the valve housing, therefore the mesh is coarser here. Region 2, 4 and 5 are transition regions consisting of tetrahedral elements. Right after the disc, the gradients of the flow variables are still high and therefore the mesh in region 4 and 5 is chosen to be finer than the mesh in region 6. Inflation layers of 3 cells are used in the pipes to get a better resolution close to the walls.

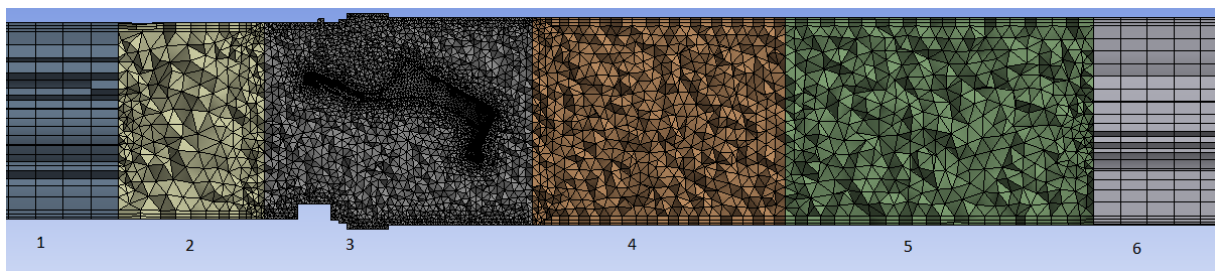


Figure 4: A cross section of the mesh.

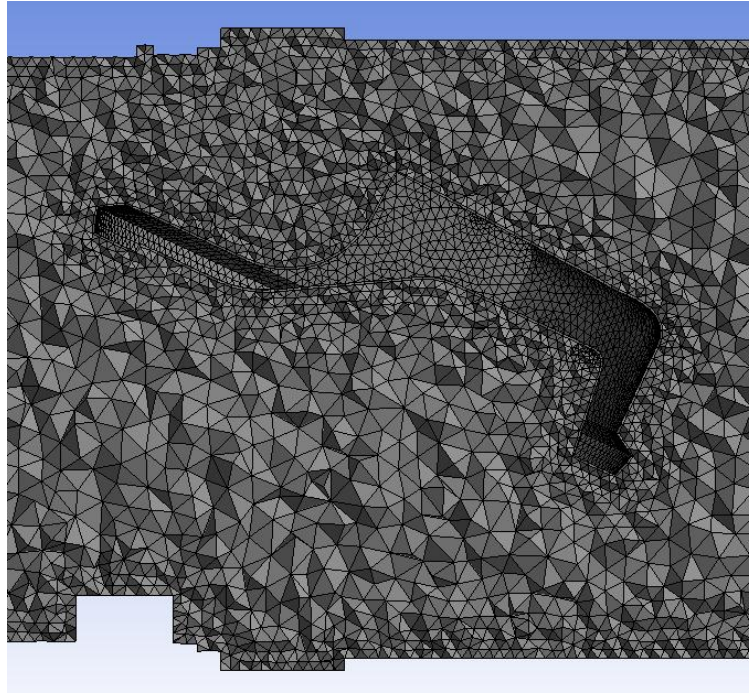


Figure 5: A close-up view of the mesh around the disc.

4.2.2 CFD simulation

Before a transient simulation, an initialization of the flow field has to be performed. In the default simulation, a hybrid initialization is first performed, where after a steady state simulation is run in 2,000 iterations. Thereafter, a transient initialization is performed in 2 s with a time step of 10 ms. In both the steady and transient initialization, the pressure at the inlet, at the outlet, and on the disc is monitored. This is done, in addition to the monitored residuals in ANSYS Fluent, in order to ensure that a stable solution is obtained after the initialization. After the initialization, the UDF is hooked and the flow time is reset to zero. The initialization for the default simulation is also used for the simulation without the removable weight.

When performing a CFD simulation, a short computational time is preferable. In the sensitivity analyses, the coarsest mesh and the largest time step gave an independent solution, and they are therefore chosen for the default simulation. The mesh of the default simulation consists of 856,835 cells while the time step is 10 ms. The turbulence model used in the default simulation is the realizable $k - \varepsilon$ model with enhanced wall treatment and the spatial discretization scheme is set to second order upwind.

The Green-Gauss Node Based method is applied for the gradient computations, since it is preferable when the mesh consists of unstructured tetrahedral cells and since it is more accurate than a cell based method. [7] [10] PRESTO! is used as the pressure interpolation scheme since it performs better for flows with swirls than the standard interpolation scheme. [7] The coupled pressure-velocity coupling algorithm is applied because it converges faster than a segregated pressure-velocity coupling algorithm. With the coupled pressure-velocity coupling scheme, a CFL number must be set. The CFL number works as a relaxation factor in each time step. A large CFL number gives a shorter computational time with the drawback of

a possible diverging solution. If the solution diverges, the CFL number can be reduced to enhance convergence. The CFL number is set to the default value of 200.

4.3 Sensitivity analysis

To ensure that the chosen settings are appropriate for the studied flow, a sensitivity analysis is performed. The properties examined during the sensitivity analysis are:

- Mesh
- Location of inlet and outlet boundaries
- Time step size
- Maximum number of iterations in one time step
- Discretization scheme
- Turbulence model

All the simulations differ with one parameter from the default case described in the previous section. After the sensitivity analyses are performed, the results are used to compare the closing time.

4.3.1 Mesh

Three different meshes are analysed to ensure that the solution obtained from the default simulation is not mesh dependent. In addition to the mesh used in the default settings, i.e. the mesh consisting of 856,835 cells, a mesh consisting of 1,032,836 cells and a mesh consisting of 1,553,707 cells are investigated. The areas that are refined in the finer meshes are region 3, 4 and 5; see Figure 4.

4.3.2 Boundary condition

In the default simulation, the length of the pipes before and after the check valve is set to 5 m. In the sensitivity analysis, pipes with a length of 7 m are used to ensure that the locations of the inlet and outlet boundary are far enough from the check valve.

4.3.3 Time step size

Three different time step sizes are investigated to ensure that the solution does not depend on the chosen time step size. The time step sizes that are investigated are 10 ms, 5 ms and 2.5 ms.

4.3.4 Maximum number of iterations in one time step

The number of iterations in each time step is analysed. In order to ensure that a maximum of 20 iterations per time step is enough to obtain a converged solution, a simulation with a maximum of 40 iterations is investigated.

4.3.5 Discretization scheme

The MUSCL discretization scheme is analysed in addition to the second order upwind scheme. The MUSCL discretization scheme can give better accuracy for swirling flow than the second order upwind scheme.

4.3.6 Turbulence model

Two different turbulence models are also investigated, the realizable $k - \varepsilon$ model, used in the default simulations, and the standard $k - \varepsilon$ model.

4.4 UDF

In this master's thesis, a UDF handles the change of the boundary condition at the inlet and controls the movement of the disc. The boundary condition at the inlet is a decreasing mass flow rate according to equation (3.1) and the movement of the disc is determined by the forces from the fluid and the gravitation.

The following DEFINE macros are used in the UDF:

- DEFINE_EXECUTE_ON_LOADING
- DEFINE_EXECUTE_AT_END
- DEFINE_CG_MOTION
- DEFINE_PROFILE

As the name suggests, DEFINE_EXECUTE_ON_LOADING performs actions when the UDF is loaded. In this master's thesis, the macro is used to name the different columns in the text file where the data is saved. DEFINE_EXECUTE_AT_END executes different actions at the end of each time step, i.e. in the last iteration. It is used for writing data to a text file and for computing the moments on the disc. The pressure and viscous forces are obtained from ANSYS Fluent, through two different macros. The DEFINE_CG_MOTION macro uses the angular velocity to change the position of the disc in every time step. The DEFINE_PROFILE macro is applied to handle the change of the inlet boundary condition.

5 Results

The result from the CFD simulations are presented in this chapter. The results from the main analyses are presented in chapter 5.1 and the results from the sensitivity analyses are presented in chapter 5.2. The aim was to fully close the valve, but unfortunately, the simulations failed with a few time steps left. The disc was positioned at different angles when the simulations failed. The simulations failed due to a negative cell volume in the mesh.

5.1 Main analysis

In Figure 6, the mass flow rate and the characteristics of the closure for the simulations with and without the removable weight are shown. Both the simulations failed before the disc was fully closed due to the negative cell volumes. 12.3 degrees and 15.6 degrees were the positions of the disc when the simulations failed. In order to obtain a closing time for the two cases, the last part of the closure has therefore been extrapolated. The closing times for the simulations with and without the removable weight were 1.06 s and 1.19 s respectively.

There is a major difference in the behaviour of the closure between the simulations with and without the removable weight. The default simulation starts to close at 0.22 s while the simulation without the removable weight starts to close after 0.73 s. The total mass of the moving parts is 30 % lower in the simulation without the removable weight than in the default simulation. The corresponding reduction in moment of inertia for the simulation without the removable weight is 82.6 %.

In Figure 7, the opening angle and the moments for the simulations with and without the removable weight are shown. Before the disc starts to move, it is held at its fully opened position. The moments due to viscous forces are very small in comparison to the moments due to pressure and gravitational forces. The moments due to pressure vary with the mass flow rate and the moments due to gravity vary with the position of the disc. The moments due to pressure forces from the fluid are larger than the moments due to gravitational forces in the beginning of the simulation, resulting in the maximal opening position of the disc.

With the predefined mass flow rate, the valve starts to move at 0.22 s for the default simulation. At this event, the net moment due to pressure forces and gravitational forces become smaller than zero. Later in the closing process, at 0.54 s, the net moments become larger than zero again, which retard the closure of the disc. At 0.75 s, this increase of the net moments results in a slight reopening of the disc; see Figure 6.

In Figure 8, swirls can be seen after the disc. The streamlines from the surface of the disc illustrate the two swirls. The swirls rotate in different directions but are not symmetric. The geometry of the tilting disc check valve is symmetric everywhere except for the arms, around which the disc rotates; see Figure 2. The asymmetry of the swirls is most likely due to the different geometry of the arms.

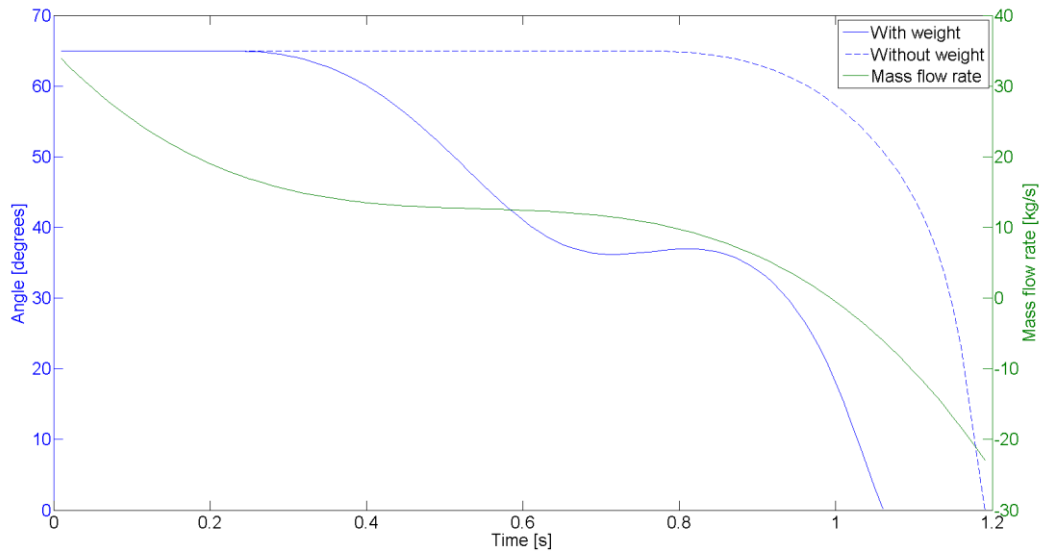


Figure 6: A plot of the opening angle and the mass flow rate versus the time. The green line represents the decreasing mass flow rate. The blue lines represent the closure of the check valve with and without a weight attached to the lever arm respectively.

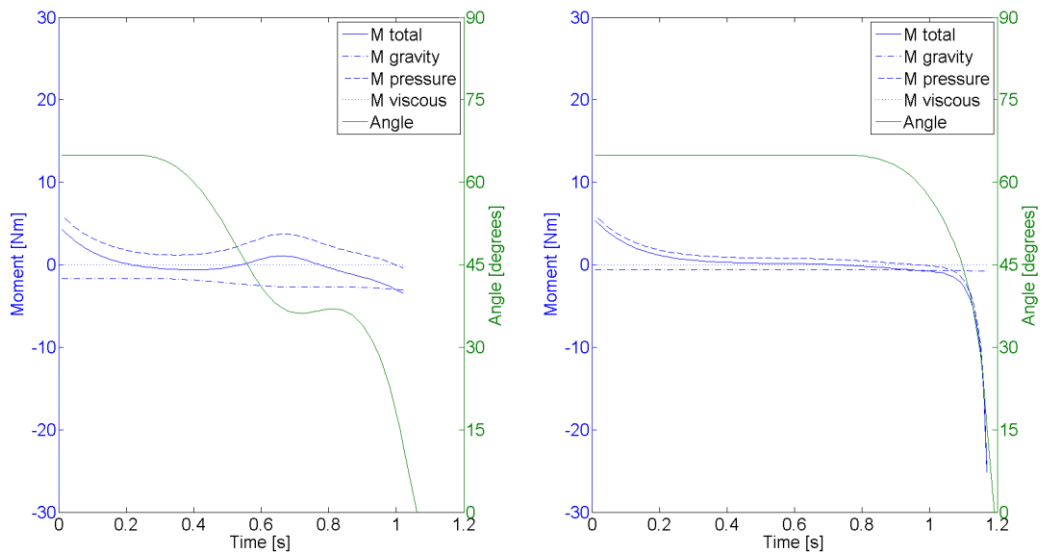


Figure 7: A plot of the moments on the disc and opening angle versus the time. The left figure represents the closure of the check valve with a weight attached to the lever arm, while the right figure represents the closure of the check valve without a weight attached to the lever arm. The green lines represent the opening angle while the blue lines represent the moments on the disc.

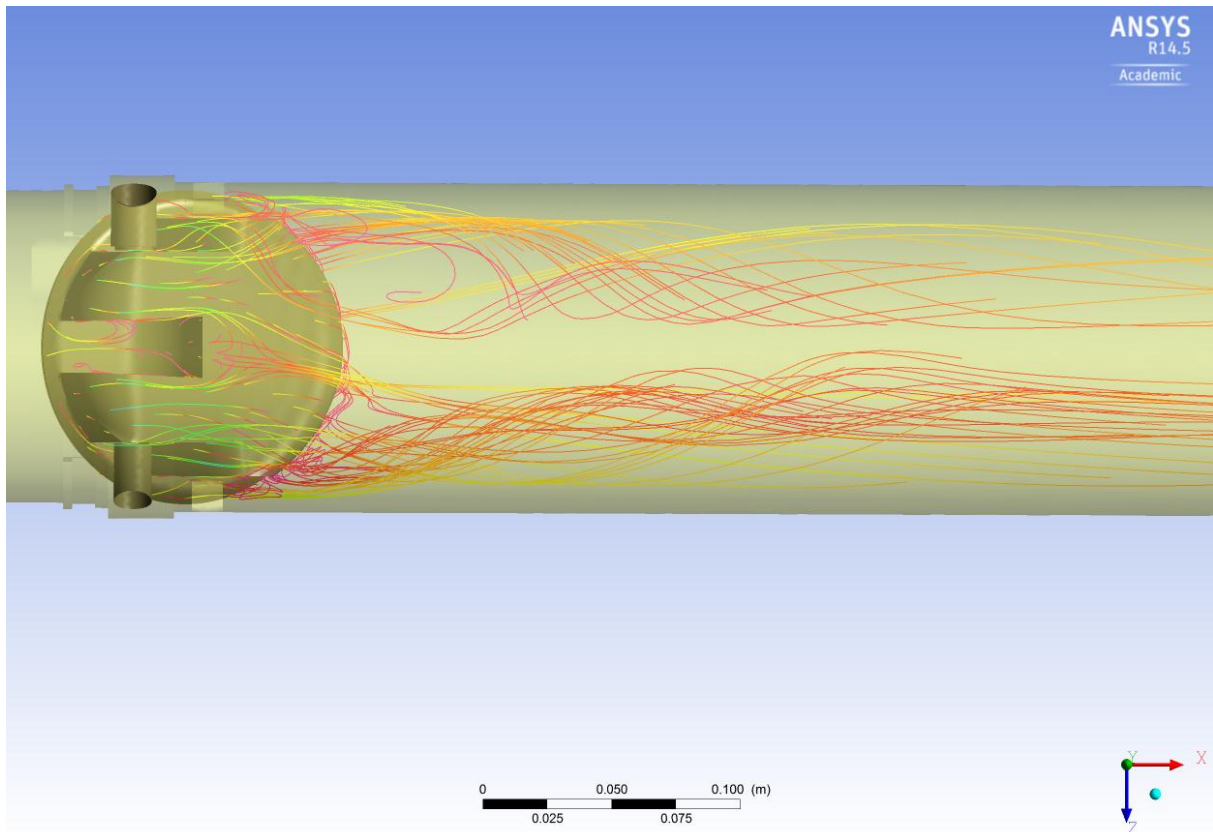


Figure 8: A picture of the streamlines behind the disc seen from above 0.2 s in the transient simulation.

5.2 Sensitivity analysis

All sensitivity analyses are compared to the default simulation and the results are presented in the following subchapters.

5.2.1 Mesh

In Figure 9, the sensitivity of the valve closure is shown for the different meshes investigated in this sensitivity analysis. There are some minor differences between the default simulation and the simulation with the two finer meshes. The behaviour of the three lines in Figure 9 is the same from 0 s to 0.6 s, while there is a slight difference at the reopening of the disc from 0.6 s to 0.8 s. In the two simulations with the finer meshes, the disc does not reopen as much as in the default simulation. When the disc continues to close, the lines coincide again.

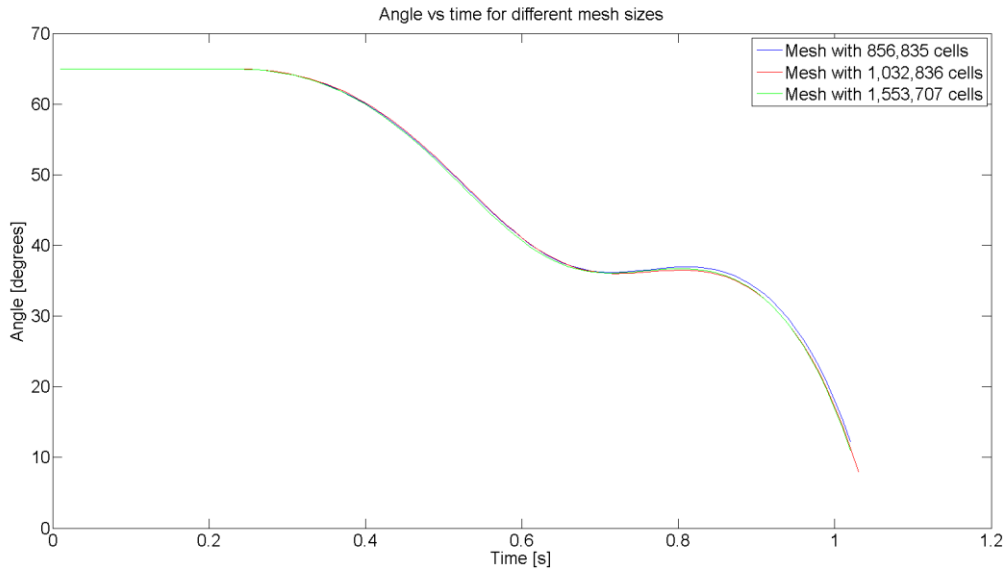


Figure 9: A plot of the opening angle versus the time for different mesh sizes. The blue line represents the closure of the disc with the mesh consisting of 856,835 cells, the red line represents the closure of the disc with the mesh consisting of 1,032,836 cells, and the green line represents the closure of the disc with the mesh consisting of 1,553,707 cells.

5.2.2 Boundary condition

The result from the CFD simulations with different pipe lengths at the inlet and at the outlet can be seen in Figure 10. The behaviours of the closure of the disc for the two different simulations are similar. The largest difference exists in the first part of the closing process. When the disc reopens, the lines start to coincide again.

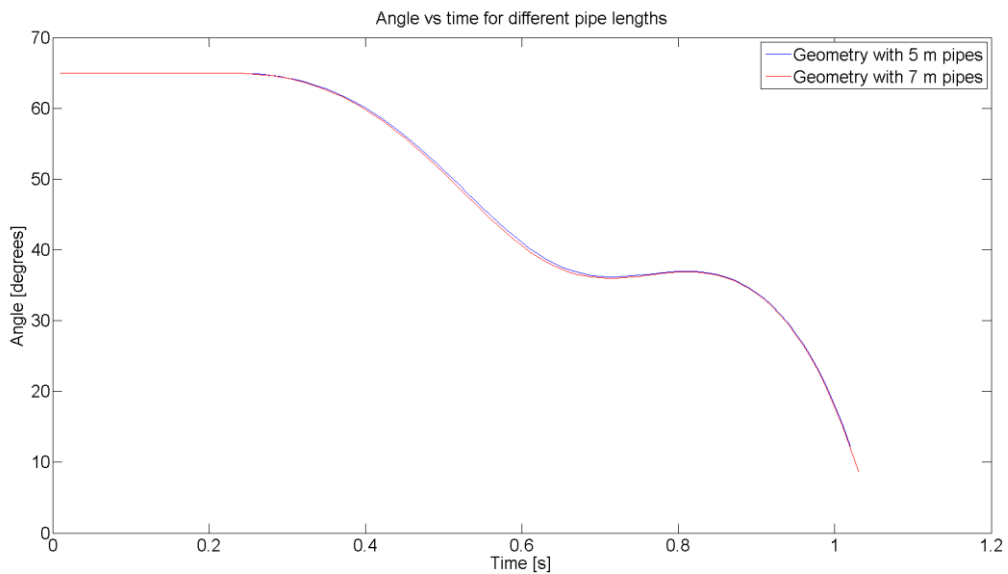


Figure 10: A plot of the opening angle versus the time for different length of the pipes before and after the check valve. The blue line represents the closure of the disc when 5 m pipes are used and the red line represents the closure of the disc when 7 m pipes are used.

5.2.3 Time step size

Three different time steps have been investigated and the results are shown in Figure 11. The lines representing the different time step sizes have the same behaviour. The smaller the time step the later the disc starts to close. The differences between the three simulations are not significant.

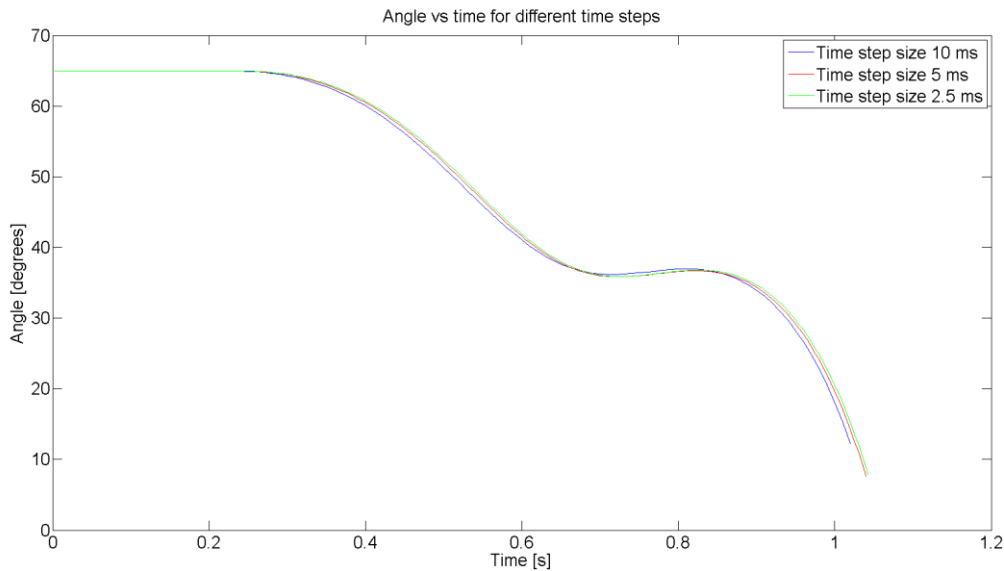


Figure 11: A plot of the opening angle versus the time for different time step sizes. The blue, red and green line represents the closure of the disc when the time step sizes are 10 ms, 5 ms and 2.5 ms, respectively.

5.2.4 Maximum number of iterations in one time step

The result from the sensitivity analysis that concerns the maximum number of iterations per time step can be seen in Figure 12. The two lines overlap throughout the simulation.

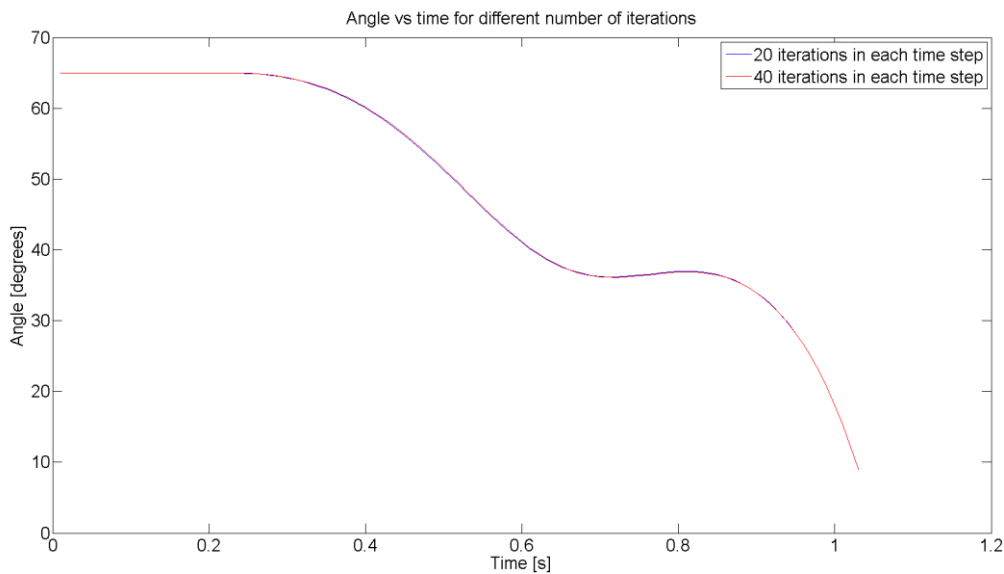


Figure 12: A plot of the opening angle versus the time for different maximum number of iterations. The blue line represents the closure of the disc when a maximum of 20 iterations are used in every time step and the red line represents the closure of the disc when a maximum of 40 iterations are used in every time step.

5.2.5 Discretization scheme

The reason for why the MUSCL discretization scheme was investigated is to resolve the swirls after the disc in a more correct manner. [9]

In Figure 13, the difference in the behaviour of the closure of the disc for the two different discretization schemes is presented. At the start, the two simulations coincide until 0.4 s where the simulation with the MUSCL discretization scheme starts to close faster. The simulation with the MUSCL discretization scheme starts to reopen the disc earlier than the default simulation. After the reopening the default simulation starts to close the disc earlier, i.e. the reopening of the disc takes longer time in the MUSCL simulation. In the reopening process, the MUSCL simulation results in a larger reopening of the disc. This is also why the MUSCL simulations have a longer closing time. In the end, the two lines in the graph start to coincide since the angular velocity of the disc for the MUSCL simulation is larger than it is in the default simulation at the same angle.

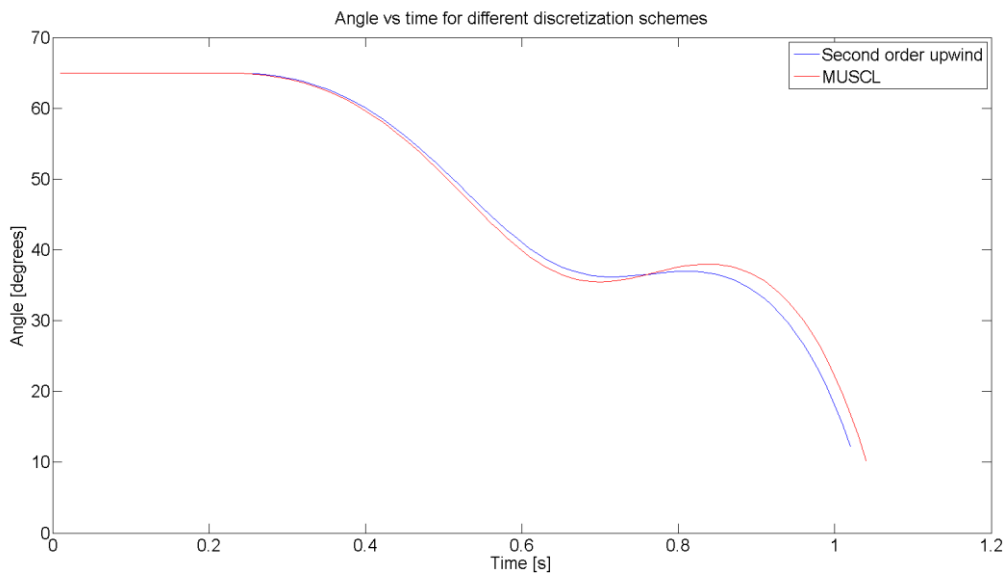


Figure 13: A plot of the opening angle versus the time for different discretization schemes. The blue line represents a simulation using the second order upwind scheme and the red line represents a simulation using the MUSCL scheme.

5.2.6 Turbulence model

The closure of the disc for the default simulation and for the simulation with the standard $k - \varepsilon$ model can be seen in Figure 14. The start and the end of the closure of the disc are similar. The behaviour of the closure is however different. In the beginning, the default simulation starts to close faster than the simulation with the standard $k - \varepsilon$ model. At the reopening process, the simulation with the standard $k - \varepsilon$ model does not open as much as the default simulations, leading to a decreasing difference between the opening angles. In Figure 15, it can be observed that the moments due to pressure forces are smaller for the standard $k - \varepsilon$ model than for the default simulation in the reopening process. This can explain the smaller rate of reopening for the standard $k - \varepsilon$ model. The reopening process starts and ends approximately at the same time for the two simulations.

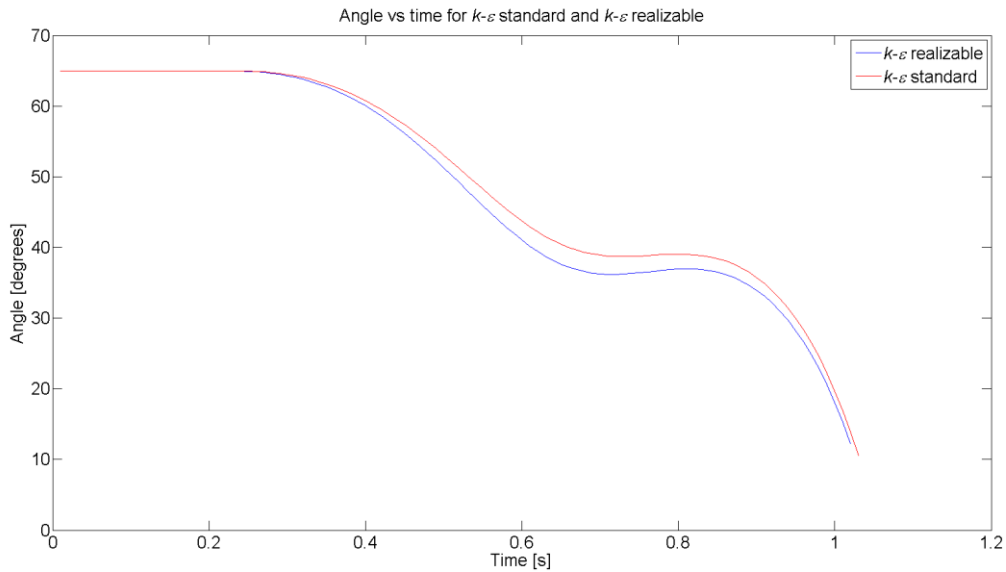


Figure 14: A plot of the opening angle versus the time for different turbulence models. The blue line represents a simulation using the realizable $k - \varepsilon$ model and the red line represents a simulation using the standard $k - \varepsilon$ model.

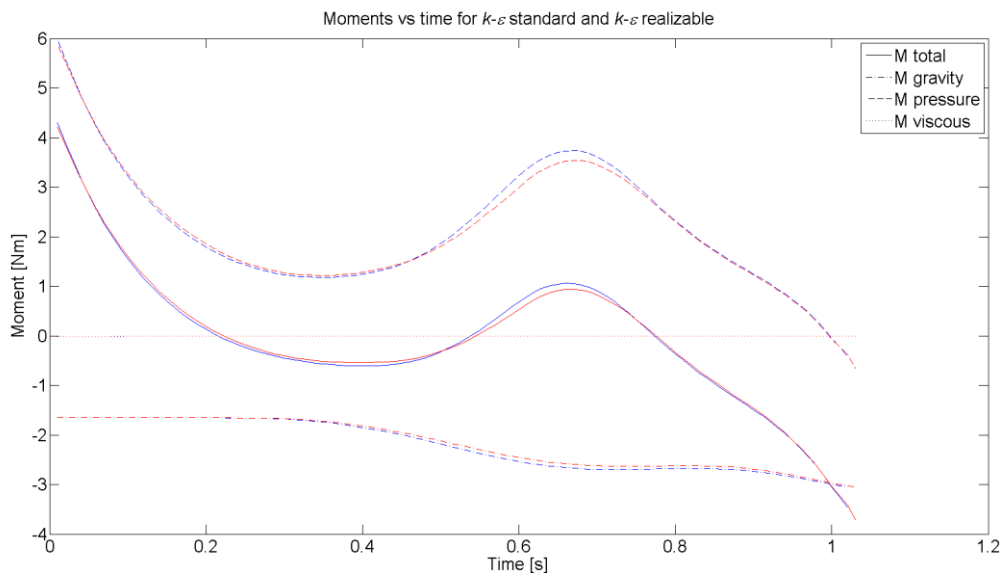


Figure 15: A plot of the moments on the disc versus the time for different turbulence models. The blue lines represent the moments in the simulation using the realizable $k - \varepsilon$ model and the red lines represent the moments in the simulation using the standard $k - \varepsilon$ model.

A dynamic pressure contour plot can be seen in Figure 16. The view is a cross section of the pipe taken 10 mm in the positive x-direction from the rotational axis, looking towards the inlet; see Figure 16. The two simulations differ in that the default simulation has larger gradients in the dynamic pressure.

In Figure 17, the turbulent viscosity can be seen for the default simulation and the simulation with the standard $k - \varepsilon$ model. The view is a cross section of the pipe taken 10 mm in the positive x-direction from the rotational axis, looking towards the inlet; see Figure 17. The default simulation shows a large difference in the gradient, especially in the middle of the

disc. One additional difference observed in the contour plots in Figure 17 is that the simulation with the standard $k - \epsilon$ model is more diffusive.

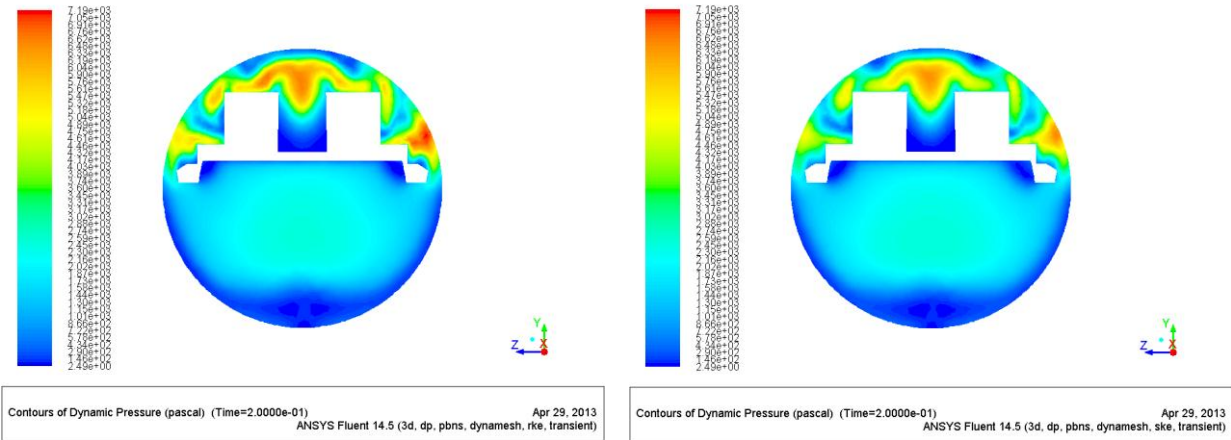


Figure 16: A contour plot for the dynamic pressure at a cross section of the pipe taken 10 mm in the positive x -direction from the rotational axis, looking towards the inlet. The contour plot was generated after 0.2 s in the transient solution. The left figure shows the contour plot from the default simulation while the right figure shows the contour plot of the standard $k - \epsilon$ simulation.

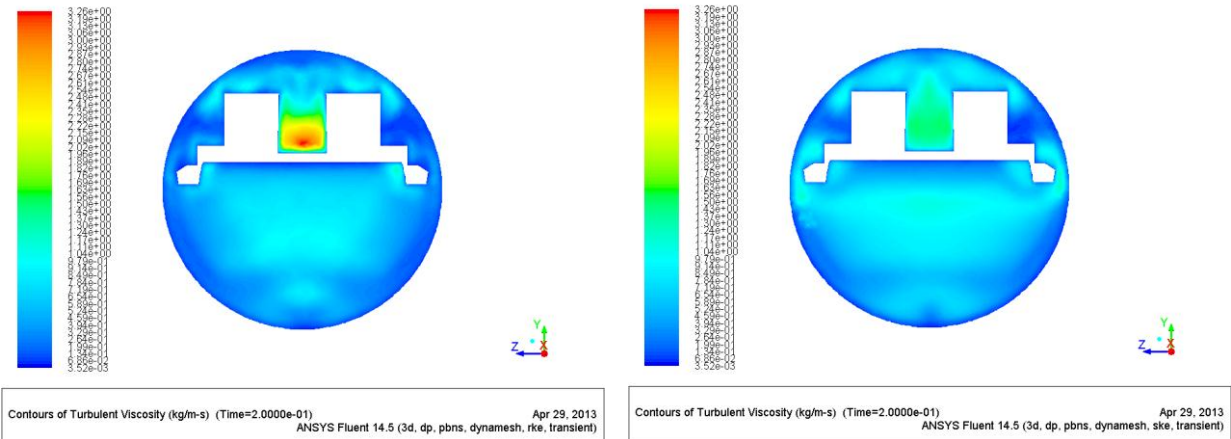


Figure 17: A contour plot for the dynamic pressure at a cross section of the pipe taken 10 mm in the positive x -direction from the rotational axis, looking towards the inlet. The contour plot was generated after 0.2 s in the transient solution. The left figure shows the contour plot from the default simulation while the right figure shows the contour plot of the standard $k - \epsilon$ simulation.

6 Discussion

All the simulations fail before the disc has reached its final position, i.e. before the disc is in full contact with the wall. This is because the disc moves too fast in comparison to the size of the cells and therefore negative cell volumes appear. The negative cell volume can be avoided by enlarging the cells at the critical area, by minimising the time step, or by a combination of both. It would still be a problem when the disc comes close to the wall because there must be one cell-layer between the two separate walls. In this case, the disc has one inflation layer that cannot be remeshed with the chosen remeshing method, i.e. there will always be a gap between the disc and the wall of at least the size of the inflation layer. In ANSYS Fluent version 14.5 an additional DEFINE macro, DEFINE_CONTACT, has been added that can be used to solve this problem. The simulation of the closure fails before this problem occurs and the new macro has therefore not been tested in this master's thesis.

In all simulations with the removable weight, the disc reopens again during a part of the closing process. How much the disc reopens, differ in the different sensitivity analyses. The mass flow rate, described in equation (3.1), decreases a lot in the beginning and in the end of the closing process. In between, the reduction of the mass flow rate is temporarily slowed down. When the reduction of the mass flow rate starts to level out, the large angular velocity of the disc, will cause the disc to pass the state were the forces on the disc are in equilibrium. The almost constant mass flow rate and the inherent inertia of the disc are thus the factors that cause the disc to pass its state of equilibrium. This passage of the equilibrium state will cause the pressure drop over the disc to increase, which eventually will cause the disc to reopen.

From ANSYS Fluent, the CFL number can be received for different parts of the fluid domain and from different time steps. The CFL is larger in the beginning of the simulation because the flow velocity is then large. The criterion for implicit scheme is that the CFL never exceeds 5 in the beginning of a simulation. The average CFL number at the start of the transient simulation is almost 3, which is fully acceptable. Every parameter that is monitored also levels out in each time step, which validates the stability further. The effect of the CFL number is more important if the explicit solver is used or if special phenomenon are to be studied. For example, to resolve pressure waves, it would be important to obtain a certain CFL number, but then the compressibility must also be taken into account.

6.1 Main analysis

The closing times and the characteristics of the simulations with and without the removable weight differ. The initial difference in the two simulations depends on the difference in the moment due to gravity for the two systems. The system with the removable weight has a larger moment due to gravity than the system without the removable weight. Therefore, the simulation with the removable weight will start to close earlier compared to the simulation without the removable weight. When the simulation without the removable weight eventually starts to close, the mass flow rate is low. When the disc has closed to an opening angle of

approximately 57 degrees, the mass flow rate reverse direction. Thereafter, the fast closure is thus due to the negative mass flow rate. In the end of the closing process, the angular velocity of the disc without the removable weight is larger than in the default simulation. A large angular velocity right before the closure can lead to large forces on the surrounding piping system when the disc slams into the wall. The mass of the disc will also affect the forces on the piping.

The mass flow rate influences the closing process; therefore, the characteristics would most likely be different with another approximation of the pump curve, or another pump curve. It would be even better with a pressure condition at the inlet, because then the water would not be forced through the pipe. Since a one-way coupling between the pump and tilting disc check valve is assumed, a simulation with a two-way coupling would probably change the results.

There are both several pros and cons with CFD simulations. For example, one advantage is that CFD simulations are cost effective compared to real experiments. One of the disadvantages is that the flow is never fully resolved, since the CFD software has built in approximations. The approximations are among others; discretization errors, round off errors, and approximations in the turbulence models. Therefore, the simulation results must be compared to experimental results.

6.2 Sensitivity analysis

In the sensitivity analyses, the results are often very similar to the default simulations when it comes to the behaviour of the disc. However, the flow may differ between the simulations without affecting the behaviour and the closing time; see Figure 16 and Figure 17.

6.2.1 Mesh

Even though the simulations in the sensitivity analyses of the mesh differ slightly in the reopening of the disc, they coincide when the time is about 1 s. The difference is so small that the simulations of the closure can be assumed to be mesh independent. Therefore, it is preferable to make the simulations with the coarsest mesh, since it will reduce the computational time. In order to reduce the computational time further, an even coarser mesh could be investigated to see if a mesh independent solution would still be obtained. Because the mesh dependency analysis showed that the result did not differ considerably between the different meshes, further refinements of the mesh in the already refined areas should therefore not improve the result significantly. However, a finer mesh close to the walls might improve the result, as this would resolve the large gradients there.

6.2.2 Boundary condition

The closing times are similar for the different length of the pipes, which indicates that the difference between the pipes of 5 m and 7 m do not influence the results. The flow can therefore be assumed fully developed in both cases. Shorter pipe lengths could be investigated to see how short the pipes can be without affecting the results, and thereby receive a mesh with fewer cells. Another way of minimizing the mesh is to cut the inlet pipe and use profiles obtained from a simulation with only the inlet pipe. Since the mesh in the pipes is structured,

the increase of cells is primary in the valve domain where tetrahedral cells are used, which is why the lengths of the pipes are acceptable.

6.2.3 Time step size

In the sensitivity analysis for the time step size there is a small difference in the behaviour of the closure of the disc. However, the influence of the time step size can be assumed small since the difference in the closure of the disc is small. When the experimental data is available, the results can be compared in order to choose a best adaptable time step size. One way of improving the characteristics of the disc could be to have different time step sizes in different parts of the closure process. It could be managed by the UDF by specifying when a new time step size shall be used. A large time step size would be used where there is no rapid change in the behaviour of the closure, while a small time step size are preferable where the changes are rapid. A small time step size could also be used in the end of the simulation when the disc approaches the wall. The combination of the smaller time step size and the use of the DEFINE_CONTACT macro may then lead to a simulation where the valve is fully closed.

6.2.4 Maximum number of iterations in one time step

In the default simulation, the maximum number of iteration in one time step is set to 20. In this sensitivity analysis, the value of 40 iterations is investigated. The results of the characteristics and the closing times are very similar for both simulations. The monitors of the pressure at the inlet, at the outlet and on the disc that is used to check the convergence, have a large change in the beginning of the time steps. After about 20 iterations, the value of the pressure level out in the different monitors in ANSYS Fluent, this explains the similarity of this sensitivity analysis.

6.2.5 Discretization scheme

The MUSCL discretization scheme was used in the sensitivity analysis of the discretization scheme, since the default simulation, that uses a second order discretization scheme, indicated that the flow is swirly after the disc. The difference in the behaviour of the closing of the disc in comparison with the default simulation could depend on the fact that the MUSCL scheme is more accurate for swirly flow. However, the MUSCL discretization scheme gives a similar closing time as the default simulation. The computational time for the MUSCL simulation is about 2.5 times larger than that for the default simulation. The default simulation can be said to be acceptable because the closing time are approximately the same for the two simulations and because the computational time are much longer for the MUSCL simulation.

6.2.6 Turbulence model

When investigating the two turbulence models in the sensitivity analysis there are some differences. The closing process of the disc is different, which originates from the differences in the derivation of the turbulence models. The turbulent viscosity is derived differently in the realizable and standard $k - \varepsilon$ models and in Figure 17, it can be seen that the two models give different results for the turbulent viscosity. The realizable $k - \varepsilon$ model is constructed in order to resolve the flow better, which is the case for the turbulent viscosity. The turbulent viscosity has a larger gradient on the top of the disc between the arms; see Figure 17. The change of the turbulent viscosity and the change of the $\varepsilon -$ equation influence all the flow variables. The

realizable $k - \varepsilon$ model also handles flows involving swirl better than the standard $k - \varepsilon$ model, which is why it is chosen in the main analysis. The static pressure is approximately the same for both the standard and realizable $k - \varepsilon$ simulation, i.e. only the dynamic pressure influences the total pressure differences. The dynamic pressure difference can be seen in Figure 16. This difference of the dynamic pressure leads to the difference of the moments of the total pressure for the standard and realizable $k - \varepsilon$ simulation; see Figure 15.

During the transient simulation, the y^+ - value at the walls changes as the mass flow rate at the inlet decreases. In the beginning of the simulation, the facet average y^+ - value in the domain is 86 and when the mass flow rate at the inlet is zero, the facet average y^+ - value in the domain is 17. Thus in the beginning of the simulation, the wall functions are preferable, but as the mass flow rate at the inlet decrease the $y^+ > 30$ criterion for the wall functions is hard to obtain without changing the near wall mesh. Therefore, the enhanced wall treatment has been used which is less sensitive to the y^+ - value, than the wall functions. A better solution would be to use a fine near wall mesh.

Another turbulence model that has been investigated in the simulations is the SST $k - \omega$ model. The initialization of the simulation did not converge. Therefore, different tests have been made in order to get a converged solution for the SST $k - \omega$ simulation. Different initializations were made in order to get convergence but the effects of the convergence were not improved. For example, the initialization of the default case was used when starting a transient simulation. A finer mesh was also tested without success. The coarse mesh was modified using the grid adaption setting in ANSYS Fluent version 14.5 for the mass continuity because the continuity equation had convergence problem.

The $k - \varepsilon$ models are constructed to apply for fully turbulent flows, i.e. in flows where the global Reynolds number is high. During the transient simulation, the mass flow rate and hence, the velocity at the inlet do decrease to zero. This implies that the global Reynolds number would also decrease and become low during the simulation. Therefore, the use of more advanced turbulence models, such as the transition model or large eddy simulation, could be investigated to see if this would generate a different closing time.

7 Conclusion

Since the CFD simulations include approximations, see chapter 6.1, the results from the main simulation must be validated to the experimental results in order for the results to be fully reliable. In the sensitivity analysis, the characteristic of the closing is slightly sensitive to the settings. The largest differences can be seen in the turbulence models and the discretization schemes. Therefore, the deviations in the sensitivity analyses for the discretization scheme and the turbulence model can further be investigated. However, the sensitivity analysis gives a similar closing time as the default simulation and is therefore robust. Hence, this implies that the closing times of the tilting disc check valve can be assumed predicted correctly with the given boundary conditions. If the mass flow rate from the experiment differ from the mass flow rate boundary condition used in these simulation the results would most probably be different. Since a mass flow rate condition forces the water through the pipes, a pressure inlet boundary condition given from the experiment would be more realistic.

8 Future work

In addition to the analyses performed in this master's thesis, other investigations can be performed to complement the study. If the results from the experiments and the simulations differ much, different actions can be performed. First, the inputs from the experiment can be checked and verified, e.g. the mass flow rate. Secondly, the assumptions in the CFD simulations can be evaluated, e.g. the incompressible flow. Thirdly, the settings in the CFD simulations can be changed, e.g. the turbulence models. However, all the changes must be motivated in order to rely on the simulations. The suggestions are presented in the list below.

- The time step size can be changed throughout a simulation. This can be carried out using an additional UDF.
- Investigate other turbulence models, for example the transition models.
- Try other discretization schemes.
- Investigate the effects of another mesh. For example, use a finer near wall resolution.
- Investigate other boundary conditions, such as applying the inlet profiles or using a pressure boundary condition.
- Investigate the effects of a compressible fluid.

The results from the CFD simulations could be used in order to improve or create new valve models in RELAP5.

9 Bibliography

- [1] A. G. Antaki, Piping and Pipeline Engineering, Design, Construction, Maintenance, Integrity, and Repair, CRC Press, 2003.
- [2] R. C. Dorf, The Engineering Handbook, Second Edition, CRC Press, 2004.
- [3] “Check Valves,” Spirax Sarco, [Online]. Available: <http://www.spiraxsarco.com/resources/steam-engineering-tutorials/pipeline-ancillaries/check-valves.asp>. [Accessed 30 04 2013].
- [4] “NAF-Check Tilting Disc Check Valves,” Flowserve, [Online]. Available: <http://www.flowserve.com/files/Files/Literature/Products/Flowcontrol/NAF/NFEPS3070-06.pdf>. [Accessed 30 04 2013].
- [5] W. Malalasekera and H. K. Versteeg, An Introduction to Computational Fluid dynamics The Finite Volume Method, Pearson Education, 2007.
- [6] L. Davidson, *An Introduction to Turbulence Models*, Göteborg, 2003.
- [7] B. Andersson, R. Andersson, L. Håkansson, M. Mortensen, R. Sudiyo and B. van Wachem, Computational Fluid Dynamics for Chemical Engineers, Gothenburg, 2011.
- [8] D. C. Wilcox, Turbulence Modeling for CFD, DCW Industries, Inc, 2006.
- [9] “ANSYS FLUENT User's Guide Release 14.5,” ANSYS Inc, Canonsburg, 2012.
- [10] “ANSYS FLUENT Theory Guide Release 14.5,” ANSYS, Inc, Canonsburg, 2012.
- [11] “ANSYS FLUENT UDF Manual Release 14.5,” ANSYS, Inc, Canonsburg, 2012.
- [12] F. M. White, Fluid Mechanics, McGraw-Hill Companies, 2003.
- [13] *Mail contact with Thomas Probert, OKG.*